UC Riverside

UC Riverside Electronic Theses and Dissertations

Title

Block Copolymer-assisted Tuning of Electron Transport in Graphene Field Effect Devices

Permalink

https://escholarship.org/uc/item/12z0p515

Author

Ghazinejad, Maziar Ghazinejad

Publication Date

2012

Peer reviewed|Thesis/dissertation

eScholarship.org Powered by the California Digital Library
University of California

UNIVERSITY OF CALIFORNIA
RIVERSIDE

Block Copolymer-assisted Tuning of Electron Transport in Graphene Field Effect Devices

A Thesis submitted in partial satisfaction
of the requirements for the degree of

Master of Science

in

Electrical Engineering

by

Maziar Ghazinejad

September 2012

Thesis Committee:

Professor Mihrimah Ozkan, Co- Chairperson
Professor Cengiz Sinan Ozkan, Co- Chairperson
Professor Kambiz Vafai

Copyright by
Maziar Ghazinejad
2012

The Thesis of Maziar Ghazinejad is approved:

Committee Co-Chairperson

Committee Co-Chairperson

University of California, Riverside

Acknowledgment

Foremost, I would like to express my sincere gratitude to my advisors Prof. Cengiz Ozkan and Prof. Mihri Ozkan, at University of California-Riverside for their support of my master research, and their patience throughout my graduate studies.

I am grateful to Prof. Kambiz Vafai in Mechanical Engineering Department for his scientific contribution, stimulating discussions, and supports.

I would like to acknowledge National Science Foundation, the UMass Materials Research Science and Engineering Center on Polymers (NSF-MRSEC), American Public Power Association (APPA-DEED), and Graduate Division of University of California-Riverside for supporting my graduate studies.

My love and appreciation go to my family, my mother Farangis Ghaziani, my father Esfandiar Ghazianejad, and my brother Mazdak, whom without their continuous care and supports I would not be able to complete my education. Maziar

Content

List of Figures vii

List of Tables xi

Chapter 1 1

1. Introduction 1

1.1 References 5

Chapter 2 8

2. Casting, Alignment, and Processing of Block Copolymer Films for Modulating Functional Nanostructures 8

2.1 Introduction 8

2.2 Annealing Strategies for Ordering and Alignment of Micro-domains in Cylindrical Diblock Copolymers 9

2.3 Fabricarion of Nanoporous BCP films, Selective Removal of Minor Block in Diblock Copolymers 15

2.4 Fabrication of Metallic Nanostructures with Diblock Copolymer Platform . 18

2.5 Top-down Pattern-assisted self-assembly of diblock copolymer 20

2.6 References 23

Chapter 3 25

3. Block Copolymers Doping Effect on Graphene Field Effect Transistors 25

3.1 Introduction 25

3.2 Fabrication of Graphene Field Effect Devices and BCP Functionalization of Graphene 28

3.3 The Effects of DiBlock Copolymer Doping on Graphene Devices Electronic Transport 30

3.4 Characterization of Chemical and Strctural Properties of Doped Graphene 43

3.5 References 47

Chapter 4 51

4. Conclusions 51

List of Figures

Figure 2-1 AFM and SEM image of a cylindrical PS-b-P2VP film with randomly organized microdomains parallel to substrate 10

Figure 2-2 AFM and SEM image of vertical alignment in cylindrical PS-b-PMMA after using a neutral brush of same polymers and thermal annealing 11

Figure 2-3 AFM image of vertical alignment of cylindrical PS-b-P4VP by solvent annealing with tetrahydrofuran vapor (THF) 13

Figure 2-4 AFM images of cylindrical PS-P4VP aligned vertically to the substrate. From top to bottom molecular weight is: 32 kg/mol , 69 kg/mol , and 166 kg/mol. 14

Figure 2-5 AFM image of the reconstructed porous PS-P4VP after 30 minute treatment with ethanol. The P4VP cylinders are removed while the PS matrix preserved. 16

Figure 2-6 AFM image of the reconstructed porous PS-PMMA after ultraviolet irradiation and dipping in acetic acid 17

Figure 2-7 Schematic of the fabrication procedure of metallic nanoparticles/nanomask via evaporation onto reconstructed diblock copolymer templates..... 19
Figure 2-8 SEM image of hexagonally-organized uniform metallic nanoparticle deposited by PS-P4VP diblock copolymer film..... 20
Figure 2-9 Schematic of the e-beam lithography assisted patterning of aligned cylindrical diblock copolymer. The blue lines illustrate e-beam exposed areas of the BCP film that are chemically modified. 21
Figure 2-10 Schematic of the procedure where substrate is topographically patterned and then coated with diblock copolymer macromolecules 22
Figure 2-11 (a) 10 μm and, (b) 3 μm AFM image of PS-b-P2VP coated on top of nanoimprint lithography patterned substrate..... 23
Figure 3-1 Schematic illustration of the experimental setup. (a) fabrication of GFET samples with back-gate; the left image shows an optical microscopy picture of a typical device and BCP coating, (b) fluorine doping of BCP coated device, (c) the cartoon of transferring BCP to GFET..... 31
Figure 3-2 (a) AFM images of PS-P4VP block-copolymers: as assembled on Si substrates; the dark dots represent hexagonally-ordered cylindrical domains (minor component, P4VP), the bright background shows the matrix (major component, PS). (b) AFM images of the BCP after a 110s of plasma exposure. (c) AFM images of BCP after a 200s plasma exposure. (d) Raman spectra of monolayer and bilayer graphene samples..... 32

Figure 3-3 (a) I_{ds}-V_g curves for a typical pristine graphene and for BCP-covered GFET devices after drying in air, (b) Typical source-drain current vs gate voltage (I_{ds}-V_g) curve of GFET covered with BCP and 5 days in vacuum desiccator change. (c) Typical I_{ds}-V_g curves for GFET devices: pristine graphene, graphene doped with polystyrene (PS), polyvinylpyrrolidone (PVP), and BCP covered graphene with high vacuum annealing at 50°C for 12 hrs. The test was carried out by putting one drop of PS or PVP solution on GFET devices. PS and PVP solution were prepared with trichloroethylene and anhydrous ethanol respectively. (d) Normalized source-drain conductance vs gate voltage (G_{ds}-V_g) curves for a graphene devices: pristine graphene, PS covered graphene, PVP covered graphene and BCP covered graphene. The source-drain bias for these measurements was 100 mV. 34

Figure 3-4 Another graphene field effect transistor I_{ds}-V_g curve. (b) typical source-drain current vs source-drain voltage (I_{ds}-V_{ds}) curves at different gate voltages. 35

Figure 3-5 Source-drain current vs gate voltage (I_{ds}-V_g) curves of control sample: GFET in air for 5min and GFET covered with BCP..... 36

Figure 3-6 (a) Source-drain current vs gate voltage (I_{ds}-V_g) curves from samples obtained after different plasma exposure times. The exposure time was accumulated. (b) Normalized source-drain conductance vs normalized gate voltage (G_{ds}-V_g) curves from graphene device after different plasma exposure times. 38

Figure 3-7 Neutrality point shift curve with different exposure time to CF_4 plasma of 14 devices. The I-V test points were 10s, 30s, 60s, 80s, 110s, 140s, 170s, 200s. 39

Figure 3-8 Typical source-drain current vs gate voltage (I_{ds}-V_g) curves of control sample of pristine graphene before (a) and after 30s CF_4 plasma treatment (b), And (c) I_{ds}-V_{ds} curves of these two smaples which show the one order increase of resistivity after 30s plasma treatment. 41

Figure 3-9 Raman spectra of graphene and fluorine doped graphene with CF4 plasma treatment for 10s. 42

Figure 3-10 F 1s XPS spectra from a blank graphene sample (red traces) and from a sample after a CF_4 plasma treatment for 10s (black traces)..... 44

Figure 3-11 Plots the XPS spectra of (a) C 1s and (b) Si 2p..... 44

Figure 3-12 Plots of the fittings for the C is XPS peak obtained from the (a) blank and (b) 10s CF_4 plasma-exposed samples. 46

List of Tables

Table 3-1 The peak positions, peak areas, and assignments obtained from blank sample fittings..... 45

Table 3-2 The peak positions, peak areas, and assignments obtained from F-doped sample fittings..... 45

Chapter 1

1. Introduction

Block copolymers (BCP) are a specific group of polymers that contain two or more of chemically distinctive and homogenous polymer segments or blocks. The polymer blocks in BCP macromolecule are covalently attached in well-defined sequence. [1-6] In the most basic case, BCPs are derived from two linearly linked segments (here labeled as block X and Y), and is referred to as X-b-Y dibock copolymers. [1-6] Adding more chemically distinctive blocks will form triblock copolymer to multiblock copolymer, which containing three or more polymer segments, respectively. In multiblock copolymers the blocks can be organized linearly or in a branched format that forms star block architecture. The possible combinations of components assemblies result in an extensively versatile types of morphologies in BCPs. As in other multi-component materials system, the distinctive, and sometimes contrasting, physical and chemical natures of building components have resulted in unique properties in block copolymers.

The significant feature of block copolymers (BCPs) is their ability to phase separate on molrcular-scale, which is termed microphase separation. [1-6] Many studies have been devoted to investigate the mechanisms by which different building blocks of BCPs separate from each other in the entire structure of BCP macromolecules. [7-14] Indeed, it is the micro-phase separation phenomenon that leads to BCPs intriguing self-assembly behaviors. Therefore, to apply the self-assembly of block copolymers it is necessary to understand microphase separation and its involving factors.

The major parameters that control microphase separation and hence final self-assembled structures in BCPs are: the nature of interaction between the building monomers, the ratio between constituent blocks, and the molecular size and conformation of each block. The first factor that determines feasibility of microphase separation is the Flory–Huggins interaction parameters, termed χ-parameter. Flory–Huggins is a thermodynamic parameter that demonstrates the incompatibility of two interacting polymers, or how much they dislike each other. [1-6] The larger positive values of χ-parameter point to stronger separation of polymer blocks in BCP, whereas, negative χ-parameter indicate that phase separation, and accordingly self-assembly does not happen. Another important factor is the polymerization degree, N, which shows how many monomers are present in each block. The summation of the individual block's polymerization degrees yields total degree of polymerization. For example, in a diblock copolymer we have: $N_{tot} = N_X + N_Y$. The polymerization degree will directly determine the size and molecular weight

of a polymer, the product of polymerization degree and Flory–Huggins parameter, χN_{tot}, is a thermodynamic measure that quantifies the extent of microphase separation, and hence, self-assembly in BCPs. [1-6] Targeted values of χN_{tot} may be achieved by appropriate choice of polymer blocks and their molecular weight.

Another factor involved in phase behavior study is the relative volume fraction that each block occupies in the entire body of a block copolymer structure. This volume fraction, also called composition, is conventionally shown by f_X and $f_Y = 1 - f_X$, for blocks X and Y respectively. [1-6] For f_X values of around 0.5 we will have a similar sizes of two polymer blocks X and Y, which results in lamellar structure. [1-8] The lamellar structure is simply made up of similar plates of polymer X and Y that are alternatively stacked. However, when the building blocks have dissimilar volume fractions, they shape into more complex morphologies. From thermodynamic equilibrium point of view, lower contacting area in interfaces of two polymer blocks is more stable. [1-6] As a result, when $f_X < f_Y$, the minor block X segregate into rounded domains within the matrix of major block Y. In the case of diblock copolymers, a spherical phase formation of minor block X in the matrix Y is observed approximate values of $f_X \approx 0.20$. [1-6, 9] The spherical micro domains of polymer X have body centered cubic structure. If the minor volume fraction changes to around $f_X \approx 0.3$, then hexagonally arranged cylinders of minor block will from in the matrix of major polymer Y. [10-14] These lattice structures of polymer blocks allow block copolymers to automatically assemble into well-organized nano/micro-scale patterns and structures; a key feature that is critical for fabrication of functional nanostructures.

In addition to the adaptable morphologies, desired functionality could be integrated to diblock copolymers by premeditated selection of constituent blocks with specific chemical functional groups.[1, 10-14] Typical examples of diblock copolymers that are currently used in nanoscale science and technology include: Polystyrene-b-Polymethylmethacrylate (PS-b-PMMA), Polystyrene-b-Polyvinylpyridine (PS-b-PnVP), and Polystyrene-b-Polyethylene Oxide (PS-b-PEO). Currently, block copolymers are more valued for their nano/micro-scale attributes (in particular their self-assembly) and their macroscopic properties are considered technologically less applicable. [1-3]

Graphene is a carbon allotrope that consisits of one-atom-thick planar sheets of carbon atoms. Having extraordinary electrical, thermal, mechanical, and optical properties, this revolutionary material eventually claimed a Noble prize in Physics. [15-22] Accordingly, a considerable amount of theoretical and experimental research has focused on investigating potential applications of graphene nanostructures in field-effect transistors, actuators, solar cells, batteries, and sensors.[23–26] Graphene holds promises for developing future nanoelectronic devices. For implementing graphene in electronics, however, a reliable method for modulating and functionalization of graphene is among the fundamental requirements. Particularly, in many electronic devices such as graphene field effect transistors (GFET), it is essential to control or modulate the electronic properties by means of doping.

In this work, we aim to demonstrate the applicability of block copolymer to selectively tune the chemical state and electronic behavior of graphene. To this end, first we discuss how to make the self-assembled BCPs application-ready through ordering of the cylindrical diblock copolymers and implementing top-down strategies to manipulate self-organizing copolymer domains. Next, we utilize the nanoscale-ordered structures of BCPs, with their two distinctive functional groups, as a mechanism to modulate the electronic properties of graphene filed effect transistors (GFETs) in a controllable way. We will describe how the unique structure of the BCPs can provide additional benefit as protective layers for GFETs, which will be advantageous for applications in sensing. This essentially will combine some fascinating attributes of two revolutionary materials of the nanotechnology world. With their versatility in morphology, chemical functionality, and electrical properties, block copolymers and graphene are emerging as the building blocks for the next-generation of functional nanostructures.

1.1 References

[1] M. Lazzari, G. Liu, and S. Lecommandoux; "Block Copolymers in Nanosciene", WILEY-VCH Verlag GmbH&Co. KGaA, Weinheim (2006)

[2] I. W. Hamley; "Developments in Block Copolymer Science and Technology", John Wiley & Sons (2004)

[3] N. Hadjichristidis, S. Pispas, G. Floudas, "Block Copolymers: Synthetic Strategies, Physical Properties, and Applications", John Wiley & Sons (2002)

[4] F. B. Calleja, Z. Roslaniec, "Block Copolymers", CRC Press (2000)

[5] I. W. Hamley; “Block Copolymer in Solution”, John Wiley & Sons (2005)

[6] B. Lindman, P. Alexandridis; “Amphiphilic Block Copolymers: Self-Assembly and Applications”, Elsevier (2000)

[7]. M. P. Stoykovich, M. Müller, S. O. Kim, H. H. Solak, E. W. Edwards, J. J. de Pablo and P. F. Nealey, Science 308 (5727), 1442-1446 (2005).

[8] S. O. Kim, H. H. Solak, M. P. Stoykovich, N. J. Ferrier, J. J. de Pablo, P. F. Nealey, Nature, 424(6947), 411-414 (2003)

[9] R. A. Segalman, A. Hexemer and E. J. Kramer, Macromolecules 36 (18), 6831-6839 (2003).

[10] S. Park, B. Kim, J. Xu, T. Hofmann, B. M. Ocko, T. P. Russell, Macromolecules, 42(4) 1278-1284 (2009)

[11] S. Park, J.-Y. Wang, B. Kim, W. Chen, T. P. Russell, Macromolecules, 40(25) 9059-9063 (2007)

[12] B. Kim, S. Park, T. J. McCarthy, T. P. Russell, Small, 3(11) 1869-1872 (2007)

[13] S. Park, J.-Y. Wang, B. Kim, T. P. Russell, Nano Lett.2009, 8 (6), pp 1667–1672

[14] S. Park, D. H. Lee, J. Xu, B. Kim, S. W. Hong, U. Jeong, T. Xu, and T. P. Russell, Science, 323, 1030-1033(2009)

[15] http://nobelprize.org., Vol. 2012, The Nobel Prize in Physics 2010

[16] K. S. Novoselov, A. K. Geim, S. V. Morozov, D. Jiang, M. I. Katsnelson, I. V. Grigorieva, S. V. Dubonos, A. A. Firsov, *Nature* **2005**, *438*, 197.

[17] K. S. Novoselov, A. K. Geim, S. V. Morozov, D. Jiang, Y. Zhang, S. V. Dubonos, I. V. Grigorieva, A. A. Firsov, *Science* **2004**, *306*, 666.

[18] Y. Zhang, Y.-W. Tan, H. L. Stormer, P. Kim, *Nature* **2005**, *438*, 201.

[19] A. K. Geim, K. S. Novoselov, *Nat. Mater.* **2007**, *6*, 183.

[20] J.-H. Chen, C. Jang, S. Xiao, M. Ishigami, M. S. Fuhrer, *Nat Nano* **2008**, *3*, 206.

[21] A. A. Balandin, S. Ghosh, W. Bao, I. Calizo, D. Teweldebrhan, F. Miao, C. N. Lau, *Nano Lett.* **2008**, *8*, 902.

[22] C. Lee, X. Wei, J. W. Kysar, J. Hone, *Science* **2008**, *321*, 385.

[23] F. Schedin, A. K. Geim, S. V. Morozov, E. W. Hill, P. Blake, M. I. Katsnelson, K. S. Novoselov, *Nat. Mater.* **2007**, *6*, 652.

[24] X. Wang, L. Zhi, K. Mullen, *Nano Lett.* **2007**, *8*, 323.

[25] J. Yan, T. Wei, B. Shao, Z. Fan, W. Qian, M. Zhang, F. Wei, *Carbon* **2009**, *48*, 487.

[26] E. Yoo, J. Kim, E. Hosono, H.-s. Zhou, T. Kudo, I. Honma, *Nano Lett.* **2008**, *8*, 2277.

Chapter 2

2. Casting, Alignment, and Processing of Block Copolymer Films for Modulating Functional Nanostructures

2.1 Introduction

This chapter discusses the development and processing techniques that are employed to utilize the self-assembly capability of block copolymers. Because of the advantageous chemical functionality of PS-b-PMMA and PS-b-PnVP, we primarily focus on well-ordered cylindrical structures of these diblock copolymers. As mentioned in the introduction, copolymers' volume fractions and molecular weight provides control over morphology and size of BCP microdomains.[1,2] Therefore, with a correct selection of these parameters BCP polymer blocks will self-assemble into a range of well-defined cylinders of minor polymer block in a matrix of major polymer block. [3-10]

2.2 Annealing Strategies for Ordering and Alignment of Micro-domains in Cylindrical Diblock Copolymers

In order to employ diblock copolymers as nano-processing template it is required to cast them into thin films with nan-sized thickness. This is usually performed by use of standards spin-coater machine to cast the prepared copolymer solution on top of a targeted substrate material. The layer thickness of the copolymer solution is controlled by the viscosity of the solution and the spin frequency of the coater (revolution per minute). [1, 2]

As the first step, we obtained solid-phase powder of PS-b-PMMA, and PS-b-P2VP, and PS-b-P4VP. The diblock copolymer powders are prepared by anionic synthetic routes and are purchased from Polymer Source Inc. and Sigma-Aldrich. All the copolymers have polydispersity below 1.1 and minor volume fraction (for PMMA or P4VP) of around 0.3. Due to the selected volume fraction the copolymer minor blocks assemble to cylindrical domains with hexagonal lattice arrangement. As discussed earlier, the periodicity and the separation distance are controlled by the molecular weight of polymer blocks. Accordingly, to obtain cylinders of smaller diameter and shorter distance one should synthesize polymer blocks of shorter chain (smaller molecular weight) during the polymerization procedure.

When a non-selective solution of diblock copolymer is used, castings of the copolymer solution onto the substrate results in BCP films with randomly organized microdomains parallel to the substrate (Figure 2-1).

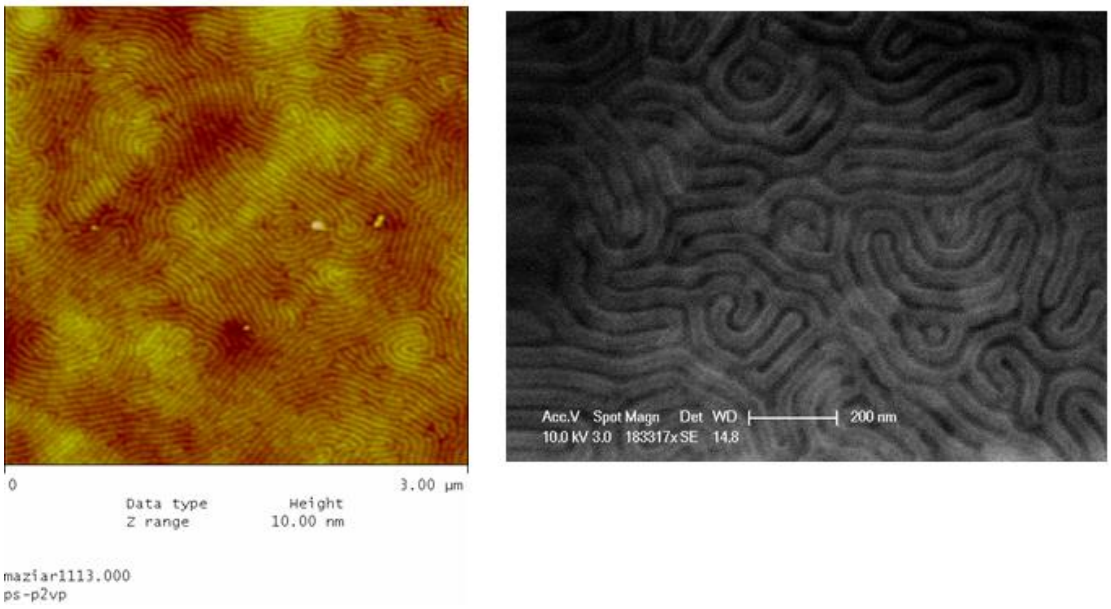

Figure 2-1 AFM and SEM image of a cylindrical PS-b-P2VP film with randomly organized microdomains parallel to substrate

Due to its unpredictable nature, this random organization limits the applicability of diblock copolymer for nano-patterning. In fact, we are interested to tilt the orientation cylindrical blocks 90 degree, thus making them perpendicular to the substrate "ground". To achieve such vertical alignment of cylindrical domains different strategies depending on the chemical and physical nature of the used polymers may be applied. One approach is to make the substrate non-selective and "indifferent" to both major and minor blocks, so that it does not "prefer" one block interface over the other one. This strategy is termed "substrate passivation", and usually involves applying a polymer brush that is neutral to the blocks used in

BCP.[1, 2, 17] This neutral brush is typically made up from random copolymers of the same monomers that form the target diblock copolymer. The neutral brush is often thermally treated after its casting on the substrate. Additionally, the diblock copolymers that are ordered by this approach are thermally annealed for additional optimization of the nanostructures. Thermal annealing usually involves controlled heating of the as-spun copolymer film in a chemically inert atmosphere or under vacuum, for a specific time. [1, 2, 17] This approach is broadly used for PS-b-PMMA diblock copolymers. In our experiments we used thermal annealing for improving the structure of the cylindrical PS-b-PMMA with molecular weight of 77kg/kmol. As shown in the figure 2-2, the surface passivation of the substrate has changed the orientation of PMMA cylinders, and organizes them vertically to the substrate.

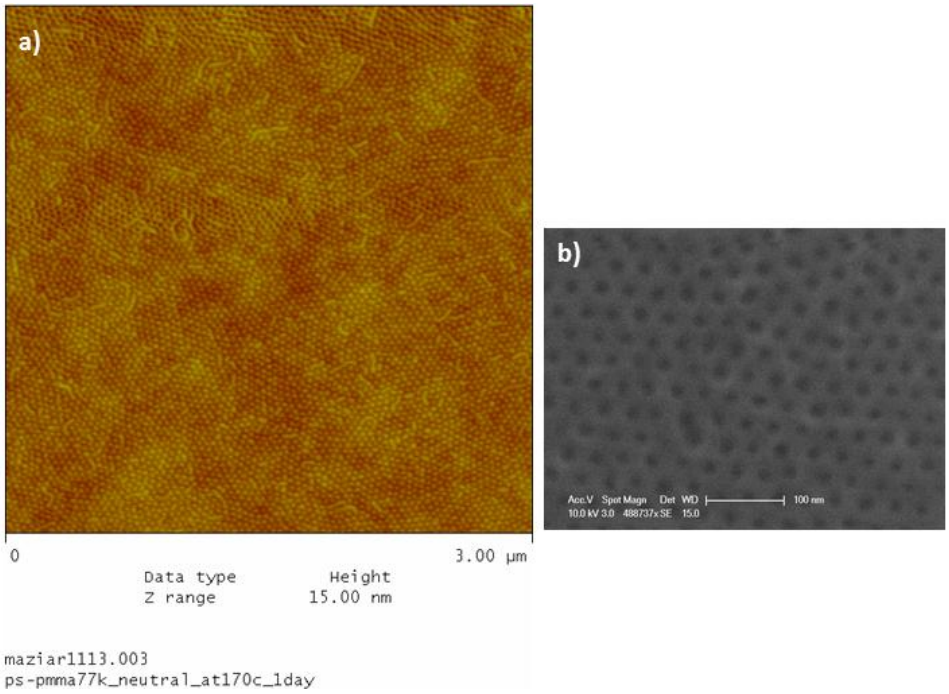

Figure 2-2 AFM and SEM image of vertical alignment in cylindrical PS-b-PMMA after using a neutral brush of same polymers and thermal annealing

Solvent annealing of BCP films is another alignment approach that has been developed and applied by Russell's group in University of Massachusetts, Amherst.[3-7] This technique generally includes exposure of block copolymer thin film to a selected solvent vapor for a carefully controlled duration. Evaporated solvent produces a directional and selective chemical field, which diffuses into BCP thin layer and restructures the minor blocks domains in the matrix of major block. Such interaction redefines the cylindrical blocks orientation and ordering. Solvent annealing has produced generally good results in ordering and alignment of PS-b-PnVP and PS-b-PEO, among other block copolymers.[3-10]

We employed solvent annealing approach to re-align PnVP cylinders in PS-b-PnVP diblock copolymers. Briefly, after casting PS-b-P2VP and PS-b-P4VP solution, the copolymer films are annealed in tetrahydrofuran (THF) vapor.[6-10] The parameters for optimized solvent annealing are highly empirical, and need to be adjusted for local ambient conditions, such as the humidity. In our first series of attempts we gained some mixed vertical alignment. The quality of theses cylindrical diblock copolymers required further improvement for the next stages of processing and polymer reconstruction. After customizing the experiment parameters to account for several involving factors, including ambient humidity, we managed to achieve full vertical alignment in cylindrical domains of PS-b-P4VP and PS-b-P2VP copolymer films. The ordering of these block copolymers are central to our studies in modulating the electronic characteristics of graphene (Figure 2-3).

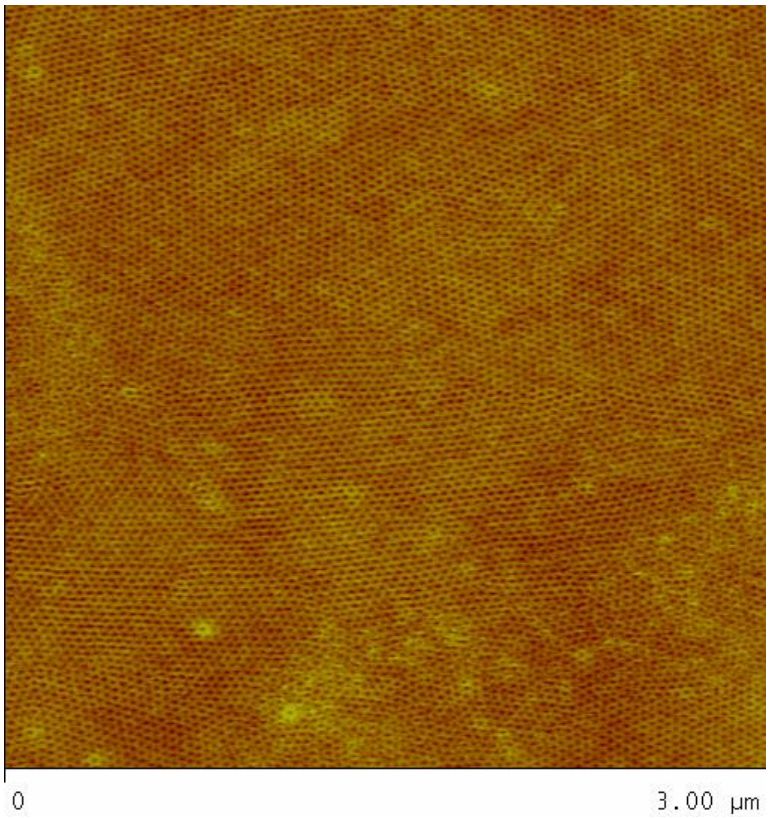

Figure 2-3 AFM image of vertical alignment of cylindrical PS-b-P4VP by solvent annealing with tetrahydrofuran vapor (THF)

The size and separation distance of the cylindrical domains can be controlled with the choice of molecular weight, or polymerization degree of the building polymer chains. To demonstrate this capability we vertically aligned cylindrical PS-P4VP with molecular weight of 166 Kg/mol, 69 Kg/mol, and 32 Kg/mol, with solvent annealing. It can be easily seen that as the molecular weight increase the diameter and spacing of the cylindrical microdomains increase.

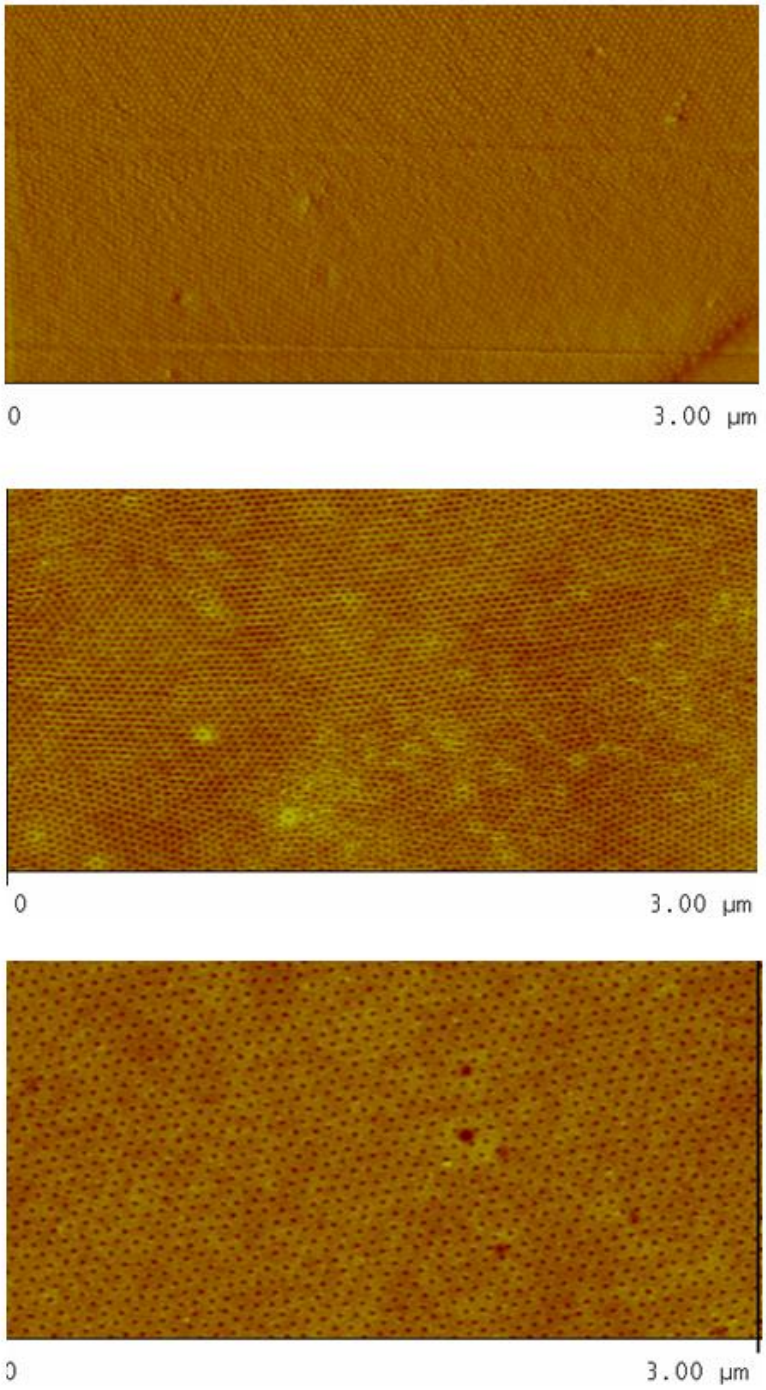

Figure 2-4 AFM images of cylindrical PS-P4VP aligned vertically to the substrate. From top to bottom molecular weight is: 32 kg/mol , 69 kg/mol , and 166 kg/mol.

In next sections of this chapter we discuss the different strategies to further process aligned cylindrical diblock copolymers thin films. These strategies include: reconstructing porous BCP membrane by selective removing of the one of the building polymers, combining top-down methods with self-assembly of BCP microdomains to achieve more sophisticated nanopatterns, and using diblock copolymers as a platform for fabrication of metallic nanoparticles.

2.3 Fabricarion of Nanoporous BCP films, Selective Removal of Minor Block in Diblock Copolymers

For many practical applications of diblock copolymer it is necessary to remove the minor cylindrical microdomain in the BCP film. This will produce a nano-porous polymer membrane with well-defined cylindrical pores embedded in the matrix of the major polymer block. The process of removing or chemically modifying one of the polymer blocks is an important nano-manufacturing technique and is termed copolymer reconstruction. Here, we focus on the experimental procedures by which the PS-b-PMMA and PS-b-PnVP block copolymer films are reconstructed.

Considering the case of P(S-b-nVP) first, copolymer reconstruction is usually carried out by immersing the vertically aligned block copolymer film in methanol and ethanol. Hydroxyl (OH) functional group in alcohols is a good solvent for PVP family and neutral to PS, therefore it can cause chain scission in P4VP domains. Note that in this reconstruction neither block of the copolymer was fundamentally

altered by the solvent and therefore the copolymer original structure may be restored by use of proper thermal treatment. For permanent removing of the chemically altered PnVP domains, the copolymer film should be exposed to a mild plasma exposure. Obviously plasma exposure would irreversibly modify both polymer blocks; however, PS much higher resilience results in a porous nanometer thick polymer film. [6-11]

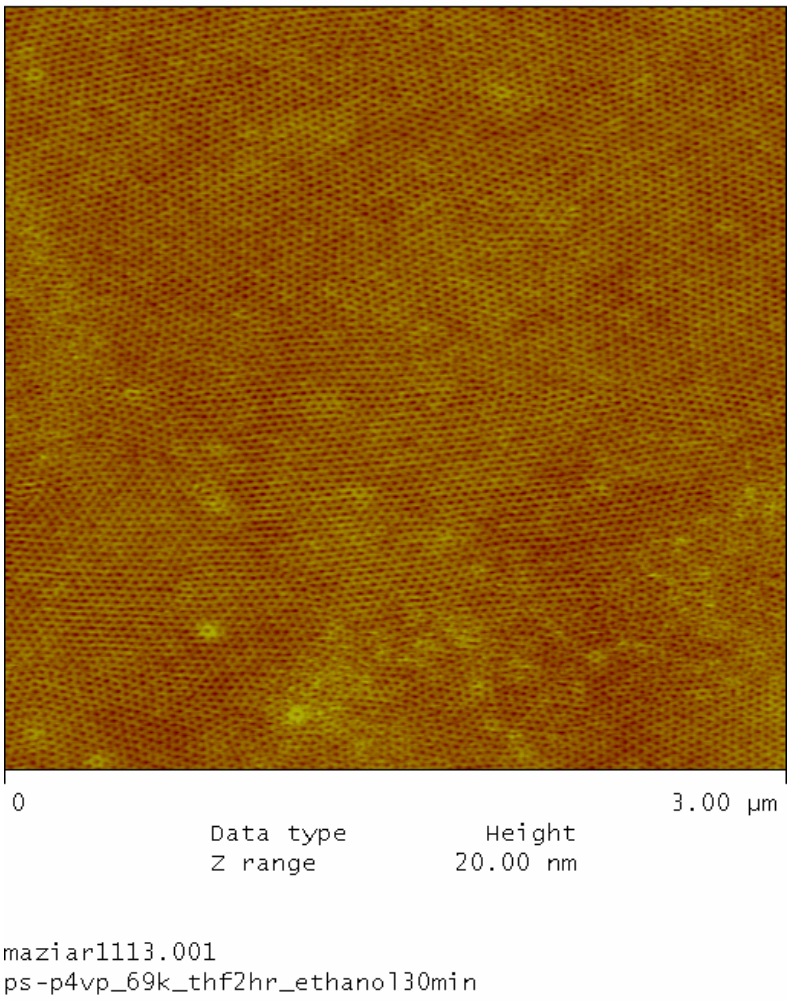

Figure 2-5 AFM image of the reconstructed porous PS-P4VP after 30 minute treatment with ethanol. The P4VP cylinders are removed while the PS matrix preserved.

The technique for removing the PMMA cylinders in PS-b-PMMA is, however, fundamentally different. Polystyrene (PS) and poly(methylmethacrylate) (PMMA) have significantly different photo-physical behaviors. PMMA a negative photoresist and when exposed to ultraviolet (UV) it goes under chain scission process. When PS is irradiated with ultraviolet, on the other hand, cross linking is the main chemical modification that happens on the structure of the polymer chains, making PS impenetrable. . The chemically altered PMMA cylinders can be completely removed via treatment with acetic acid. As a result, a premeditated UV treatment of vertically aligned PS-b-PMMA, followed by acid treatment, yields a porous PS matrix. [1-4]

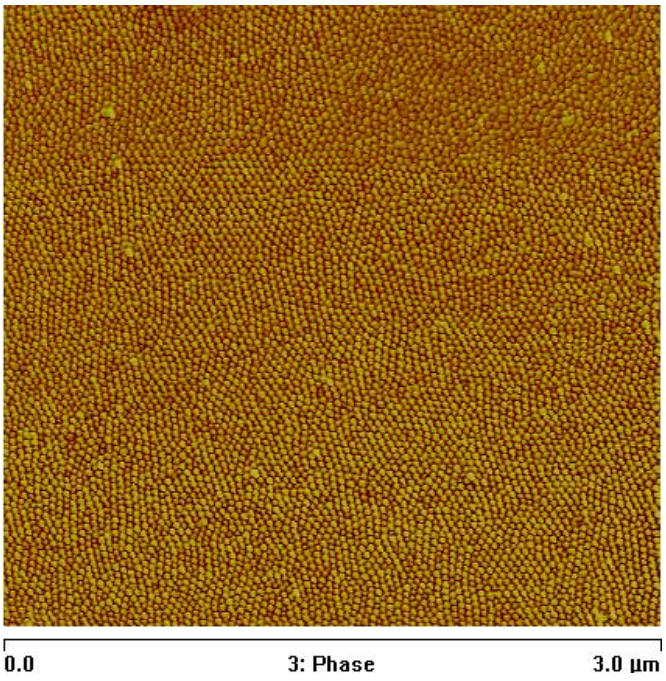

Figure 2-6 AFM image of the reconstructed porous PS-PMMA after ultraviolet irradiation and dipping in acetic acid

2.4 Fabrication of Metallic Nanostructures with Diblock Copolymer Platform

Metallic porous mask or lattice of nanoparticles can be manufactured with metal evaporation on reconstructed diblock copolymer films. This approach includes two main steps: evaporation of target metal on top of nano-porous cylindrical copolymer film, followed by etching of the polymer matrix (lift-off). Through the lift-off step the metallic nanoparticles on the copolymer matrix are removed, whereas those particles which are deposited inside the grooves or holes, are in direct contact with the substrate and withstand the lift-off processing (Figure 2-7). By inversing the volume fraction of the polymer blocks (i.e., f_{PS} = 0.3 instead of f_{PMMA} = 0.3), the same technique may be used to produce a porous metallic mask.[9]

Additionally, arrays of metallic nanoparticles can be fabricated via selective incorporation of metallic ion into the cylinders of a diblock copolymer film. In this chemical method, copolymer film is dipped in the solution of the desired metallic salt ions, such as Ni^{+2}, Fe^{+3}, Cu^{+2}, Au^{+3} and Co^{+2}.[9,10, 12-14] The chemical nature of the minor block guarantees selective absorption of the catalytic ions to cylinders and not to the matrix (major block) in BCP film. [10-12-14] Upon this loading step, dry exposure techniques, including irradiation with electron beam, ultraviolet light, or plasma treatment are applied to chemically reduce the catalyst ions and remove the

BCP film. Figure 2-8 shows SEM image of the hexagonal arrays of gold particles that are fabricated by 59K PS-b-P4VP film. Au^{+3} ions are incorporated into P4VP cylinders of the solvent annealed PS-b-P4VP by dipping the copolymer film in a 2 wt.% $HAuCl_4$ ethanol solution. The Au^{+3} loaded diblock copolymer film is then treated with 90 seconds of reactive ion etching (RIE) oxygen plasma to reduce gold ions and remove polymer film, resulting in nano-scale ordered arrays of hexagonally packed gold nano particles (Figure 2-8).

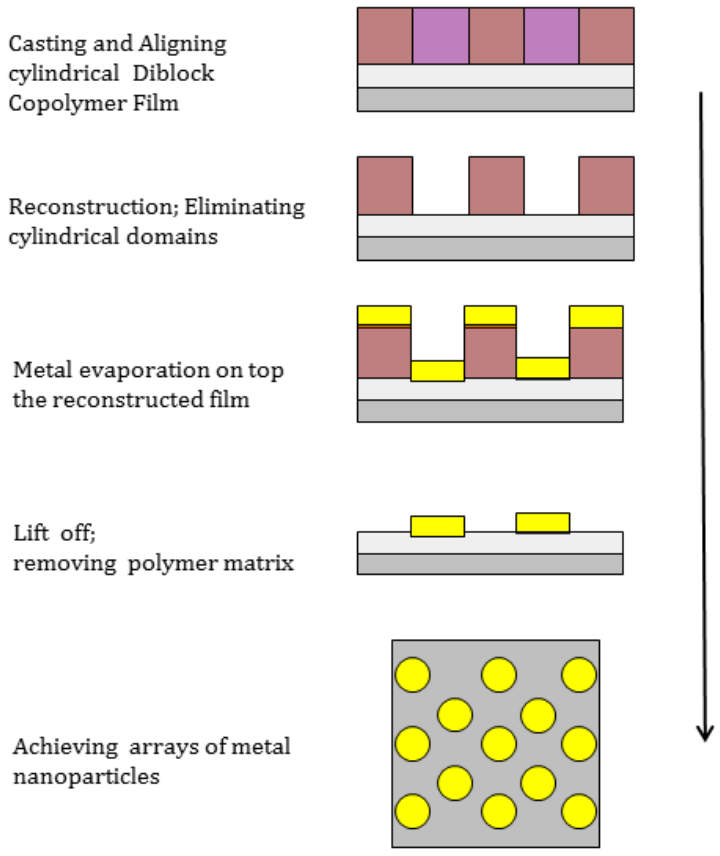

Figure 2-7 Schematic of the fabrication procedure of metallic nanoparticles/nanomask via evaporation onto reconstructed diblock copolymer templates

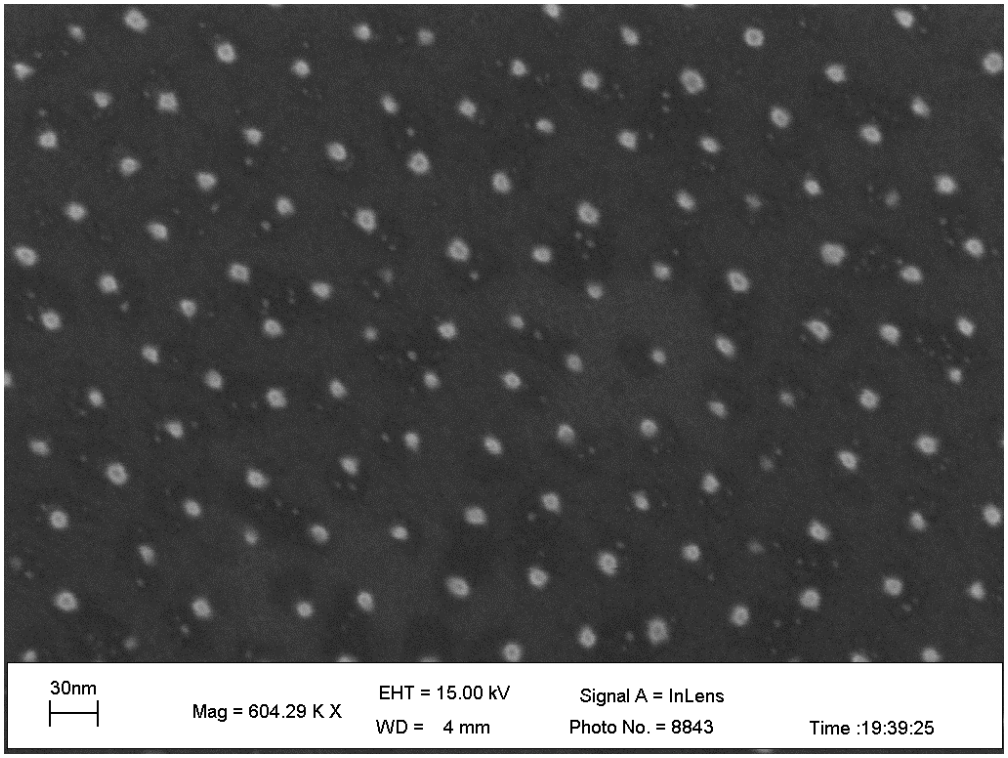

Figure 2-8 SEM image of hexagonally-organized uniform metallic nanoparticle deposited by PS-P4VP diblock copolymer film

2.5 Top-down Pattern-assisted self-assembly of diblock copolymer

Pattern assisted self-assembly is a combination of bottom-up with top-down strategies that can provide a practical approach to achieve complex nanoscale features. [11-16] In the final section of this chapter we want to discuss two practical pattern-assisted self-assembly approach for development of target functional nanostructures. The first method involves selective exposure of ordered cylindrical diblock copolymers to electron beam. [11, 13] Briefly, vertically aligned cylindrical

copolymer films, which could be previously loaded with metallic ions, is irradiated with e-beam in target locations. The cylinders that are exposed to electrons are chemically altered and are "pinned" to the substrate while non-exposed cylinders can be lifted-off by treating with appropriate solvents (Figure 2-9).

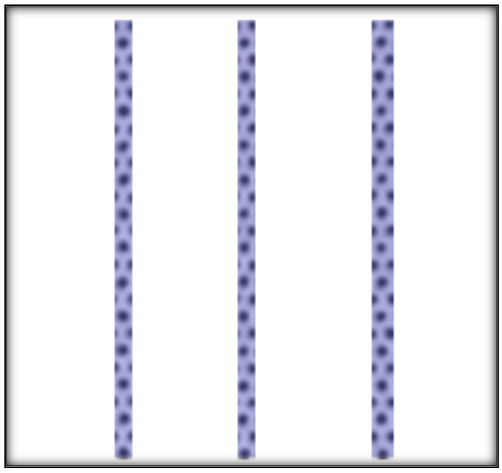

Figure 2-9 Schematic of the e-beam lithography assisted patterning of aligned cylindrical diblock copolymer. The blue lines illustrate e-beam exposed areas of the BCP film that are chemically modified.

Here, self-assembly phenomena in block copolymers provides control over size and separation distance of catalyst particles along the patterned lines, while conventional lithography meets the demand of controlled structure location of nanostructures with arbitrary separation distance. [11, 13]

Another approach implemented for large-scale nanopatterning is to employ Nanoimpring Lithography (NIL) for topographical patterning of the substrate. In this method first the topography of the substrate is designed and patterned by NIL templates. PS-b-P2VP and PS-b-P2VP copolymer solutions are then coated onto this

patterned substrate (Figure 2-10). The copolymer films can then be loaded with transition metal ions, such as Fe^{+3} and Cu^{+2}. [12-14]

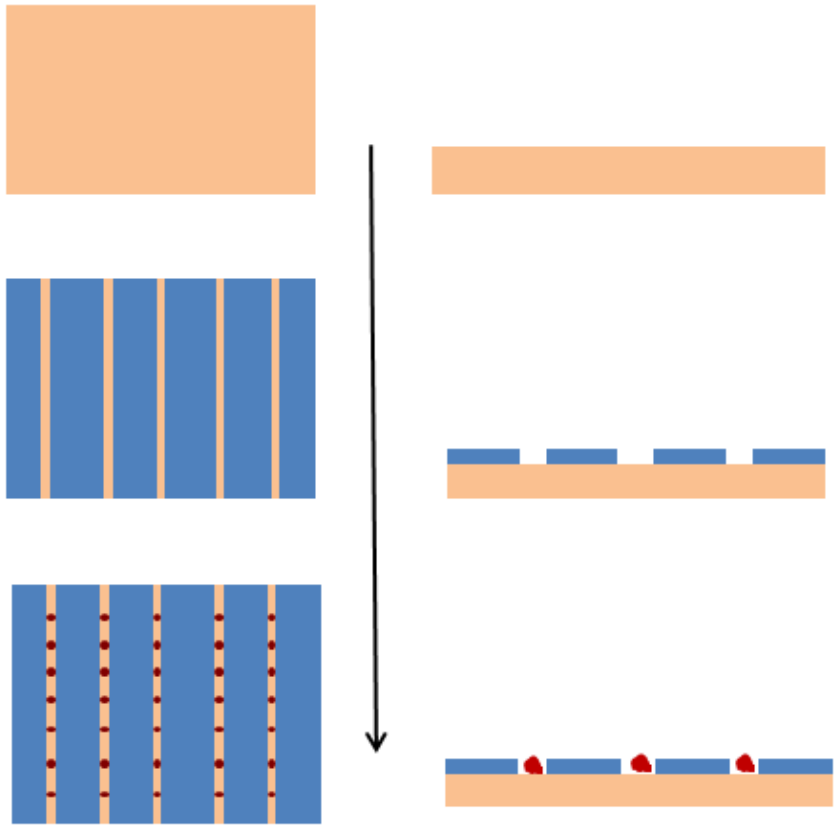

Figure 2-10 Schematic of the procedure where substrate is topographically patterned and then coated with diblock copolymer macromolecules

Figure 2-11 shows AFM image of NIL patterned substrate that is coated with PS-b-P2VP diblock copolymer film. The metallic ions can be later chemically reduced with plasma treatment, resulting in patterned lines of well-organized and uniform metallic nanoparticles.

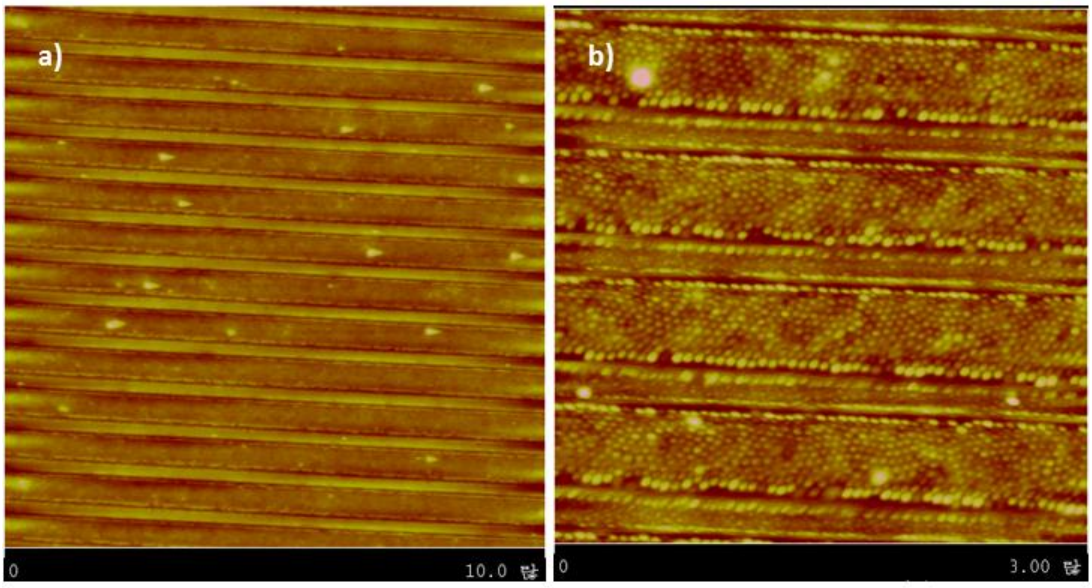

Figure 2-11 (a) 10 μm and, (b) 3 μm AFM image of PS-b-P2VP coated on top of nanoimprint lithography patterned substrate

2.6 References

[1] M. Lazzari, G. Liu, and S. Lecommandoux; "Block Copolymers in Nanosciene", WILEY-VCH Verlag GmbH&Co. KGaA, Weinheim (2006)

[2] I. W. Hamley; "Developments in Block Copolymer Science and Technology", John Wiley & Sons (2004)

[3] T. Thurn-Albrecht, J. Schotter, G. A. Kästle, N. Emley, T. Shibauchi, L. Krusin-Elbaum, K. Guarini, C. T. Black, M. T. Tuominen and T. P. Russell, Science 290(5499), 2126-2129 (2000).

[4] T. Thurn-Albrecht, R. Steiner, J. DeRouchey, C. Stafford, E. Huang, M. Bal, M. Tuominen, C. J. Hawker and T. P. Russell, Advanced Materials 12(15), 787 (2000).

[5] S. Park, B. Kim, J. Xu, T. Hofmann, B. M. Ocko, T. P. Russell, Macromolecules, 42(4) 1278-1284 (2009)

[7] S. Park, J.-Y. Wang, B. Kim, W. Chen, T. P. Russell, Macromolecules, 40(25) 9059-9063 (2007)

[8] B. Kim, S. Park, T. J. McCarthy, T. P. Russell, Small, 3(11) 1869-1872 (2007)

[9] S. Park, J.-Y. Wang, B. Kim, T. P. Russell, Nano Lett., 8 (6), pp 1667–1672(2009)

[10] S. Park, D. H. Lee, J. Xu, B. Kim, S. W. Hong, U. Jeong, T. Xu, and T. P. Russell, Science, 323, 1030-1033(2009)

[11] S. Park, O. Yavuzcetin, B. Kim, M. T. Tuominen, T. P. Russell, Small, 5(9) 1064–1069 (2009)

[12] J.P. Spatz, V.Z.-H. Chan, S. Mößmer, F.-M. Kamm, A. Plettl, P. Ziemann, M. Möller, Advanced Materials, 14(24), 1827-1832 (2002).

[13] R. Glass, M. Arnold, E. A. Cavalcanti-Adam, J. Blümmel, C. Haferkemper, C. Dodd and J. P. Spatz, New Journal of Physics 6 (1), 101 (2004).

[14] G. Kästle, H.-G. Boyen, F. Weig, G. Leng, T. Herzog, P. Ziemann, S. Riethmüller, O. Mayer, C. Hartmann, J.P. Spatz, M. Möller, M. Ozawa, F. Banhart, M.G. Garnier, P. Oelhafen, Advanced Functional Materials, 13(11), 853-861(2003).

[15]. M. P. Stoykovich, M. Müller, S. O. Kim, H. H. Solak, E. W. Edwards, J. J. de Pablo and P. F. Nealey, Science 308 (5727), 1442-1446 (2005).

[16] S. O. Kim, H. H. Solak, M. P. Stoykovich, N. J. Ferrier, J. J. de Pablo, P. F. Nealey, Nature, 424(6947), 411-414 (2003)

[17] M. Di Ventra, S. Evoy, J.R. Heflin Jr., “Introduction to Nanoscale Science and Technology”, Springer (2004)

Chapter 3

3. Block Copolymers Doping Effect on Graphene Field Effect Transistors

3.1 Introduction

Graphene has attracted a lot of attention due to its remarkable intrinsic electronic properties.[1] The ballistic transport of electrons, along with mobilities exceeding 15 000 $cm^2/V{\cdot}s$ and an ambipolar field effect, make graphene a promising candidate for the next generation of semiconductor devices.[2] Charge carrier transport in graphene can be tuned between hole and electron conduction by shifting the Fermi level with an applied electrical field.[3-5] Having the ability to accurately control charge carrier transport and spatially modulate the charge carrier density will provide a significant capability for future graphene nanoelectronics.

The materials presented in this chapter are based on our previous publications: Guo, Ghazinejad et al., **Small, DOI: 10.1002/smll.201101611**; Copyright © 2012 WILEY-VCH Verlag GmbH & Co. KGaA, Weinheim

Several methods have been developed to achieve this goal, including band gap engineering by fabricating graphene nanoribbons[6-8] or nanomeshes,[9] utilizing bilayer graphene[10] to obtain a narrow band gap, and doping of graphene layers to obtain n-type or p-type materials.[11, 12] Doping or chemical functionalization is another approach for modifying the electronic properties of graphene. Modulating the charge carrier densities provides a tuning of the Fermi level, hole and electron mobilities and a shift of the Dirac neutrality point. Several surface doping approaches with different materials have been utilized to modify the electronic properties of graphene, including metals (Ca, Ag, Au, Ti, Bi, K, etc.),[13-15] aromatic molecules,[16] poly(ethylene imine),[17] non-metal elements (N, B, etc.),[18-20] semiconductors or nanoparticles,[21] and aryl groups.[22] Meanwhile, side or edge doping has been demonstrated to exert an important role in altering the bandgap of graphene nanoribbons[23] as well as in obtaining graphene field effect transistors (GFETs) with higher on/off ratios[24] and higher electron and hole mobilities.[25] In spite of all these advances, it is still a great challenge to achieve controlled tuning of the electronic properties of graphene. A better way to partially dope graphene with specific molecules using a controllable method is needed to support further developments in fabricating novel graphene nanoelectronics. In this paper, we report on the use of di-block copolymers (BCP) for this purpose.

The ability of BCPs to assemble into ordered arrays of spheres, cylinders, and lamellae structures make them attractive templates and scaffolds for nanopatterning.[26,27] The unique structure of BCPs, with their chemical functional

groups in one chain, is likely to provide a viable mechanism for tuning the electronic properties of GFETs. Moreover, the ordered structure with two distinctive functional groups provides a means to achieve partial doping in a controllable way. We will describe how the unique structure of the BCPs can provide additional benefit as protective layers for GFETs, which will be advantageous for applications in sensing.

Recently GFETs have attracted attention for potential biochemical sensing applications. Several studies have demonstrated the high sensitivity of sensors resulting from the intrinsic properties of graphene, in applications such as pH measurements,[28] DNA detection,[29,30,46] and gas[31,32] sensing. However, the sensitivity of GFETs has in some cases proven to be inferior to that of other sensors, instabilities and unreliability of the device were observed in other cases, and low electrical responses for intrinsic graphene based devices were shown in certain examples.[33] It would be highly desirable to develop GFET sensors with higher sensitivity and reliability. The hexagonal domain structure of BCP provides heterogeneous nanoscale patterns for achieving spatially selective sensor architectures.

In this chapter, we report a block-copolymer doping effect on graphene layers, and demonstrate control of the neutrality point shift in GFETs by fluorine doping via CF_4 plasma processing. The ordered structure of the BCP enables the tuning of electron transport in graphene layers and devices.

3.2 Fabrication of Graphene Field Effect Devices and BCP Functionalization of Graphene

Synthesis of graphene: CVD graphene was synthesized using a copper foil as the catalyst.[43] Typically, the copper foil is etched with acetic acid at 35°C for 10min to remove any CuO. After washing the foil completely with deionized (D.I.) water, the copper foil samples are then heated up to 1000°C in a 2 Torr Ar/H_2 (200:200 sccm) atmosphere and annealed for 30 minutes. Following exposure to methane (100sccm) mixed with 20 Torr H_2 flowing at 1000°C for 20 minutes, the temperature is then reduced to 25°C at a cooling rate of 20 °C/min, during which the graphene film is formed on the copper surface. The residual copper foil underneath is then etched in $FeCl_3$ aqueous solution (0.5M) and rinsed thoroughly with HCl (3%) and D.I. water, respectively. The graphene film is finally transferred onto a Si substrate covered with 300nm thermally grown oxide for further characterization.

Fabrication of graphene based field effect devices: CVD grown large-area graphene sheets are patterned and etched by oxygen plasma to rectangular shapes using photolithography and a Reactive Ion Etch (RIE) system. Two terminal devices with Ti/Au (2nm/80nm) electrodes (shown in the inset of Figure 1) are then fabricated. The device is evaporated with back gate Ti/Au (2nm/100nm). The

distance between the source and drain in the devices are set to 70μm, and the width of the patterned graphene layer is 50 μm.

Fabrication of PS-P4VP block copolymer: The block copolymer used in this study is Poly(styrene-b-4-vinylpyridne) (PS-b-P4VP), purchased form Polymer Source, with a molecular weight of 69kg/mol (M_n, PS = 51 kg/mol, M_n, PVP = 18 kg/mol) and a molecular weight distribution of M_w/M_n = 1.15. The block copolymers are dissolved in toluene/tetrahydrofuran at room temperature to make 0.6 wt% polymer solutions, which are subsequently spin-coated at 2200 rpm onto silicon wafers with 300nm thermally grown silicon dioxide on it. In order to develop well-defined, well-ordered cylindrical microdomains in the BCP films, appropriate volume fractions and molecular weights are selected. The choices of volume fraction and molecular weight provide control over the morphology (cylindrical in this case) and size/separation distance in the BCP microdomains. Using the above-mentioned data, BCP domains spontaneously assemble into a range of well-defined cylinders of a minor polymer block, in a matrix of major polymer blocks. BCP cylindrical domains are then vertically aligned on the substrate by using a solvent annealing technique. This can provide a very simple but robust route to generate almost defect-free microstructures over large areas in block copolymer thin films.

Characterization*:* Raman spectra were taken using a Renishaw micro-Raman spectrometer with a 488 nm visible laser as the excitation source. Atomic force microscopy (AFM) was conducted using a Multimode-5 Veeco instrument operated in the tapping mode using standard silicon cantilevers. The XPS data were obtained

using an EA11-MCD system equipped with an Mg–Kα X-ray source (1486.6 eV) and a 100 mm concentric hemispherical electron energy analyzer.[44] All of the XPS peak positions were referenced to the graphene C 1s peak at 284.6 eV and the surface concentrations are calculated from the respective peak areas using reported atomic sensitivity factors.[45]

3.3 The Effects of DiBlock Copolymer Doping on Graphene Devices Electronic Transport

Figure 1 outlines the procedures for doping and BCP layer transfer. After device fabrication, BCP layers were transferred onto the device (Figure 1c). Briefly, the as-assembled copolymer films were peeled off from the Si/SiO_2 substrate using 1wt% HF solution. The polymer film was then collected with graphene substrate and BCP microdomains were transferred onto synthesized fabricated graphene device. This technique is similar to the TEM sample preparation of metal loaded block copolymers.[34]

The whole sample was then preserved under vacuum at 40^oC overnight so that polymer film can relax properly on the graphene. The patterned BCP was assembled according to well known protocols: typically, the Poly(styrene-b-4-vinylpyridne) (PS-b-P4VP) BCPs are dissolved in toluene/tetrahydrofuran at room temperature to make a 0.6 wt% polymer solution that is subsequently spin-coated at 2200 rpm onto a silicon wafer with 300 nm thermally grown silicon dioxide. The as-spun

copolymer films are then exposed to tetrahydrofuran vapor at room temperature for 180 min using a solvent annealing technique.[34] In this process, exposure of thin films of BCP microdomains to saturated solvent vapor increases the mobility of the copolymer micelles and results in the redistribution of those BCP microdomains.[35-37]

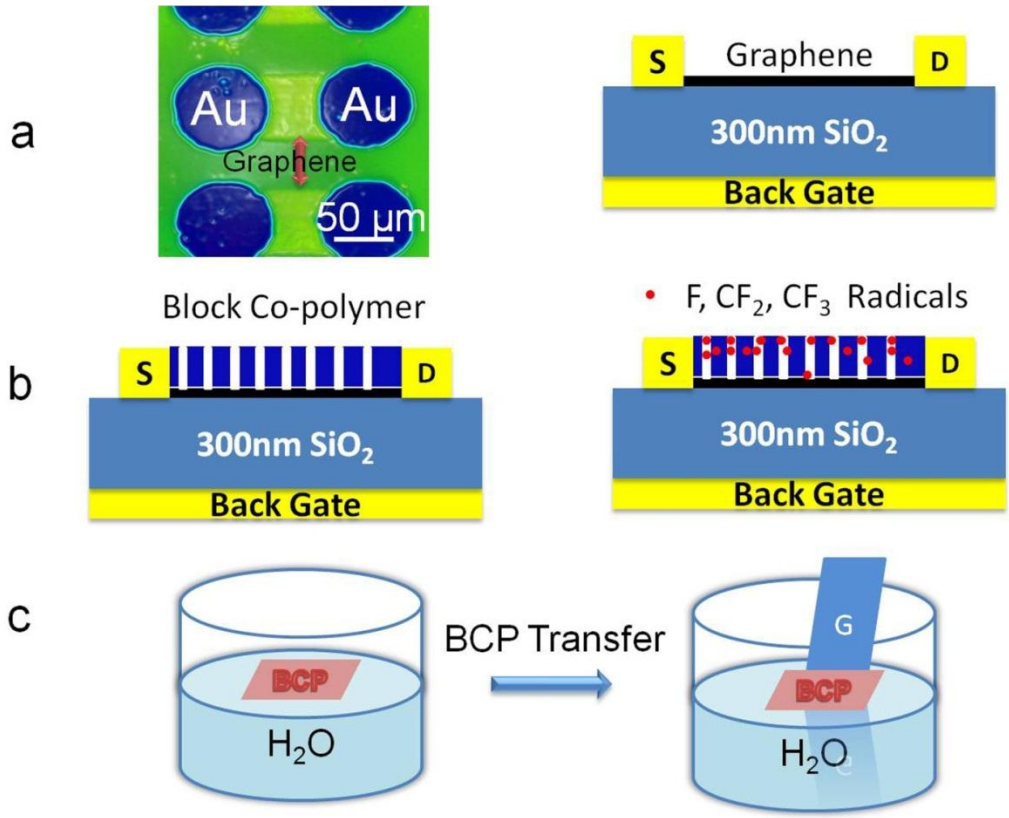

Figure 3-1 Schematic illustration of the experimental setup. (a) fabrication of GFET samples with back-gate; the left image shows an optical microscopy picture of a typical device and BCP coating, (b) fluorine doping of BCP coated device, (c) the cartoon of transferring BCP to GFET. [47]

Atomic force microscopy (AFM) images (Figure 3-2a) confirm that arrays of hexagonally ordered P4VP cylinders, with a typical dimater of ~ 30nm were

organized after annealing. The two different functional groups, i.e. benzyl and pyridine, are expected to induce a doping effect to the GFET device. To substantiate this assumption, individual polymers (P4VP and PS) and as-formed BCP film were transferred onto GFETs as shown in Figure 1, and the current-voltage (I-V) measurements were obtained. All the I-V measurements were carried out with a HP 4155C semiconductor parameter analyzer at room temperature.

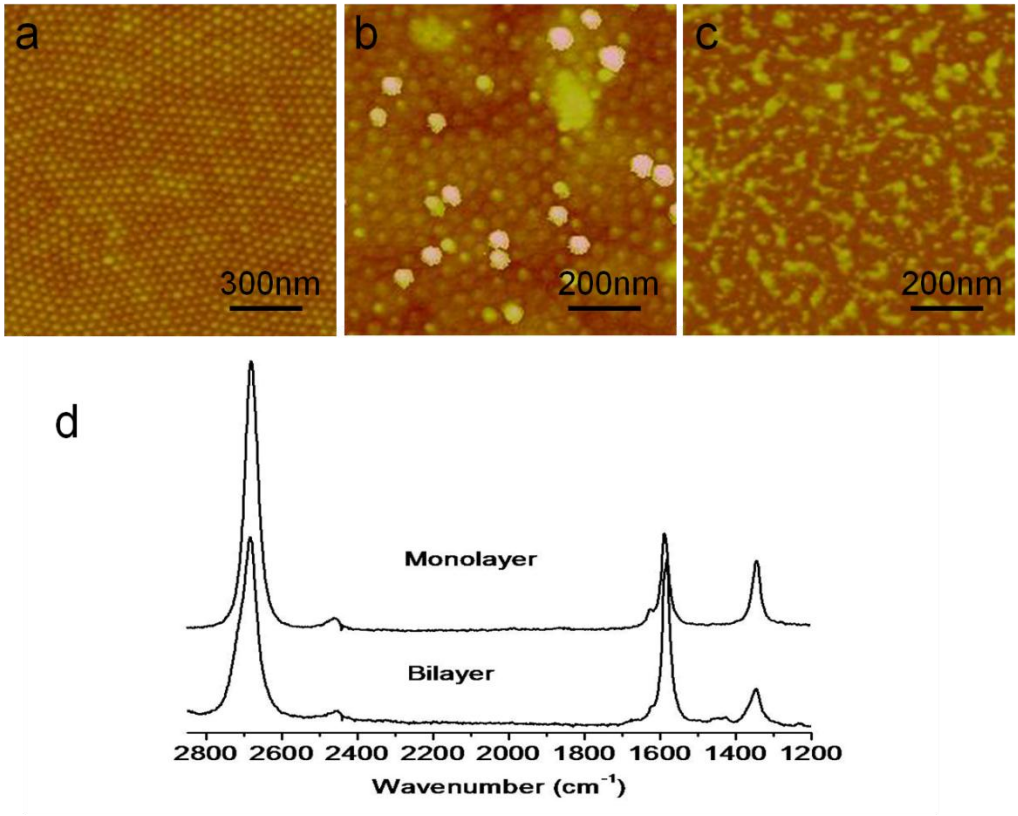

Figure 3-2 (a) AFM images of PS-P4VP block-copolymers: as assembled on Si substrates; the dark dots represent hexagonally-ordered cylindrical domains (minor component, P4VP), the bright background shows the matrix (major component, PS). (b) AFM images of the BCP after a 110s of plasma exposure. (c) AFM images of BCP after a 200s plasma exposure. (d) Raman spectra of monolayer and bilayer graphene samples. [47]

Large-area graphene sheets were synthesized via a CVD method using copper foil as the catalyst. Raman spectra obtained from our samples indicate that the graphene sheets used here have only one or two layers (Figure 3-2d). Figure 3-3a shows a typical I_{ds}-V_g curve obtained from a GFET, indicating a low defect density in the as-synthesized graphene. Average values of hole and electron mobilities were calculated as μ_{hole}= 685 $cm^2/V{\cdot}s$, and μ_e= 425 $cm^2/V{\cdot}s$ respectively. Hole and electron mobilities reach as high as 1500 $cm^2/V{\cdot}s$ and 852 $cm^2/V{\cdot}s$ respectively (Fig.S1a), indicating the high quality of the as-grown graphene, and the Ohmic contact properties of the fabricated devices (Fig.S1b) also attest to this fact. However, the charge carrier transport properties of graphene could easily be changed by exposure to air even for a short time. An experiment with a control sample showed that 5 min of exposure to air shifts the neutrality point up to +7V (Fig. S2). This phenomenon was ascribed to the doping effect of water molecules to graphene surfaces.[1] Remarkably, the neutrality point shifts to right by +20V after BCP was transferred onto the GFET (Figure 3-3a).

After 5 days of drying in a vacum dessicator, only a tiny shift in the neutrality point was observed (Figure 3-3b). However, high vacuum annealing at 50^oC for 12hrs showed that neutrality point of BCP covered GFET shifted to zero which indicates that the previous results were probably caused by a small amout of water molecules trapped between BCP and graphene sheet[38]. Interestingly, the hole and electron mobilities were increased and decreased respectively.

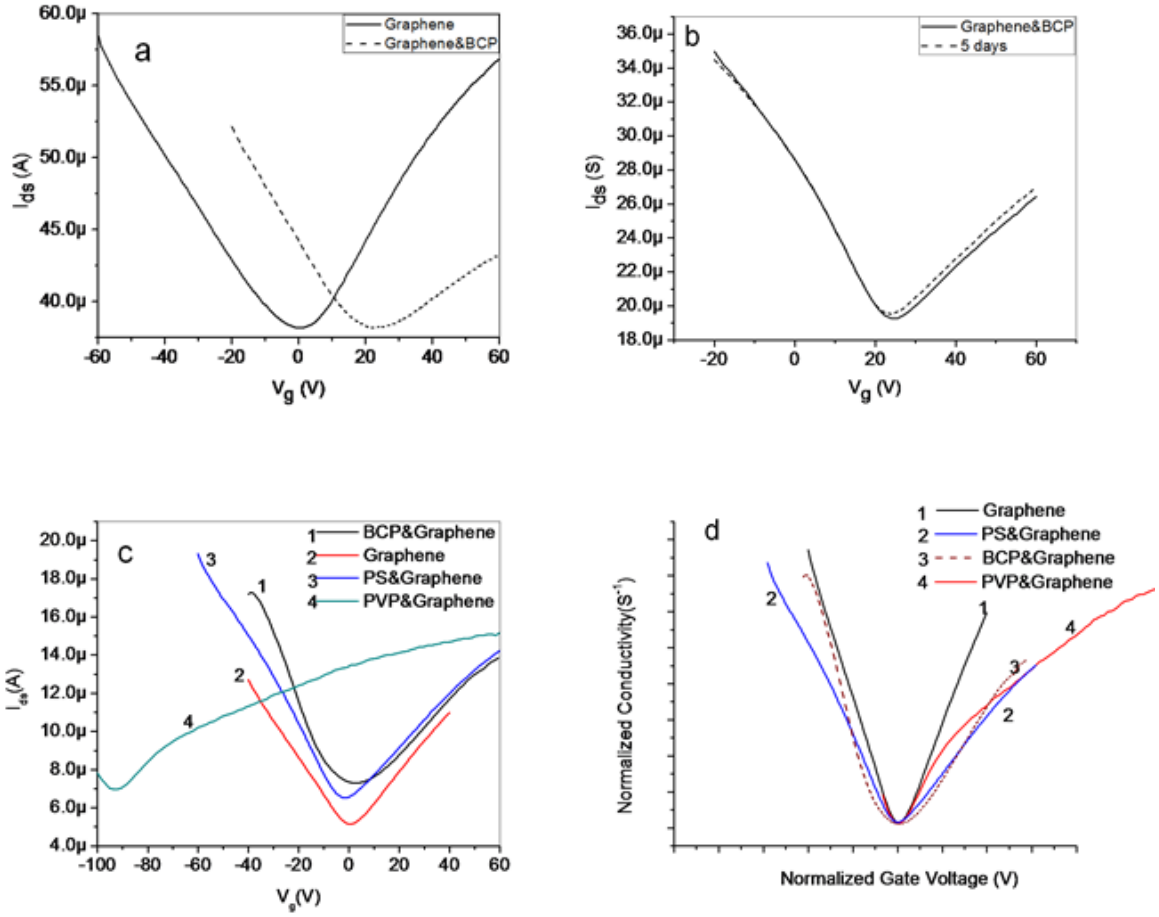

Figure 3-3 (a) I_{ds}-V_g curves for a typical pristine graphene and for BCP-covered GFET devices after drying in air, (b) Typical source-drain current vs gate voltage (I_{ds}-V_g) curve of GFET covered with BCP and 5 days in vacuum desiccator change. (c) Typical I_{ds}-V_g curves for GFET devices: pristine graphene, graphene doped with polystyrene (PS), polyvinylpyrrolidone (PVP), and BCP covered graphene with high vacuum annealing at 50°C for 12 hrs. The test was carried out by putting one drop of PS or PVP solution on GFET devices. PS and PVP solution were prepared with trichloroethylene and anhydrous ethanol respectively. (d) Normalized source-drain conductance vs gate voltage (G_{ds}-V_g) curves for a graphene devices: pristine graphene, PS covered graphene, PVP covered graphene and BCP covered graphene. The source-drain bias for these measurements was 100 mV. [47]

To further understand the doping role of BCP's polymer blocks, i.e. P4VP and PS, the doping effects were investigated individually for these homopolymers. Figure3-3c shows the I_{ds}-V_g curves of GFET covered with P4VP and PS on the surface. It

clearly demonstrates a left shift of the neutrality point after P4VP was patterned on the surface of graphene which shows a n-type doping effect. Both the electron and hole mobilities decreased for PS and PVP which may be caused by short range scattering. [17] However, having PS on the surface of graphene doesn't change the neutrality point, indicating no doping effect via PS patterning. Furthermore, the minimum conductivity was increased for all the polymers, especially for BCP doped GFET. It has been reported that minimum conductivity generally decreases by improving the homogeneity of the samples,[39] and inhomogeneous potentials created by short-range scatterers cause suppression of conductivity for both carrier types.[17] Thus, the result demonstrates the inhomogeneity of the sample upon transferring the polymer onto the graphene surface.

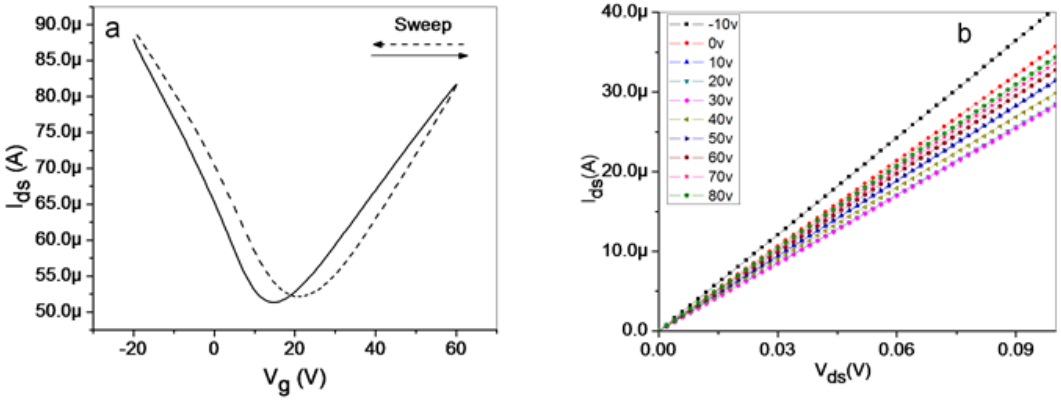

Figure 3-4 Another graphene field effect transistor I_{ds}-V_g curve. (b) typical source-drain current vs source-drain voltage (I_{ds}-V_{ds}) curves at different gate voltages. [47]

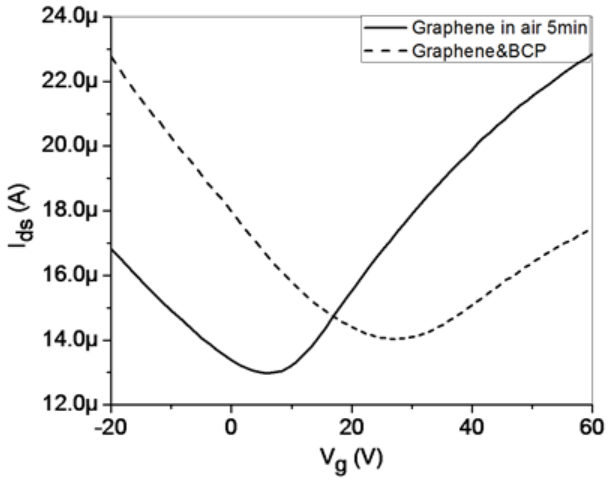

Figure 3-5 Source-drain current vs gate voltage (I_{ds}-V_g) curves of control sample: GFET in air for 5min and GFET covered with BCP. [47]

Prerviously, asymmetric electron and hole conduction branches after doping were observed for GFETs using the doping effect of poly(ethylene imine) (PEI).[17] In our case, the hole conduction was slightly increased while the electron conduction was largely supressed (Figure 3-3d), so the two branches display a different pattern compared to the case observed with PEI doped GFETs.[17] Both PS and P4VP decreased the conductivity of electron branch caused by short range scattering (Figure 3-3d), while they acted different for hole conduction. P4VP provides an n-type doping effect while the electron conduction was suppressed indicating short range scattering, causing a decrease in electron mobility. The estimated volume ratio of P4VP/PS in the present BCP is 0.73 with varying coverage areas on the graphene surface resulting in spatially different transport properties. This result suggests a good approach to change the concentration of holes and electrons with

this spatially selective doping effect. The electron and hole mobilities were calculated using the following equation:

$$\mu = [(\Delta I_{ds}/V_{ds}) \times (L/W)]/C_{ox}\Delta V_g \quad (1)$$

where L and W are the channel length and width, respectively, C_{ox} is the silicon oxide gate capacitance (which is 1.08×10^{-8} F/cm^2 for a gate oxide thickness of 300 nm), and I_{ds}, V_{ds}, and V_g are the drain–source current, the drain–source voltage, and the gate voltage, respectively.

To further control the neutrality point shift of the device, a simple fluorine doping method was introduced. Briefly, all of the BCP-covered devices were fluorinated in a reactive ion etching (RIE) machine. The plasma treatment was carried out at room temperature with the CF_4 gas pressure fixed at 10 mTorr with different exposure times, while the CF_4 flow rate was kept constant at 50 sccm, and graphene fluorination was performed with an RF power level of 25W. It has already been shown that carbon materials can be doped with fluorine by exposure to a CF_4 plasma,[40] and fluorine doping of graphene oxide (and its subsequent substitution by an amine group) has been recently reported.[41] Also, Duan et al.[9] have reported a graphene nanomesh novel structure with BCP as the template. They demonstrated that PS and PVP have different sensitivity to treatments with O_2 plasma, enabling the nanomesh fabrication.

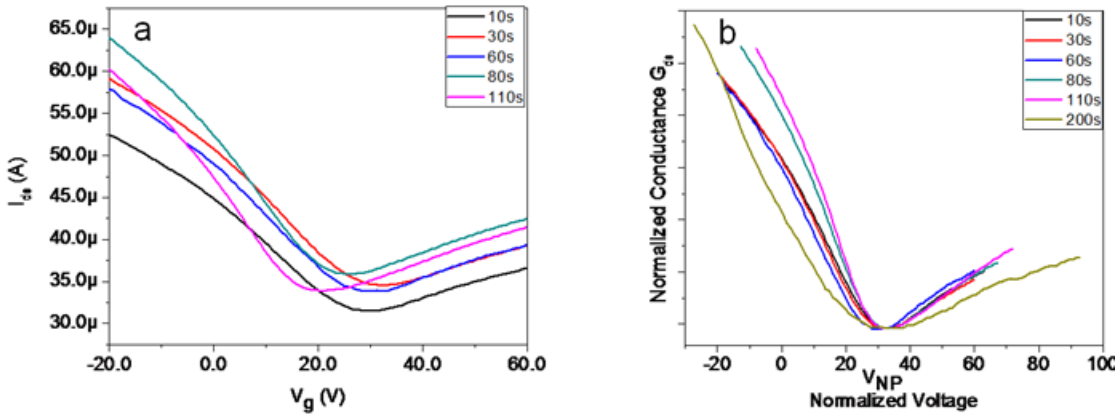

Figure 3-6 (a) Source-drain current vs gate voltage (I_{ds}-V_g) curves from samples obtained after different plasma exposure times. The exposure time was accumulated. (b) Normalized source-drain conductance vs normalized gate voltage (G_{ds}-V_g) curves from graphene device after different plasma exposure times. [47]

Here we speculated that such a difference might be utilized in doping BCP-protected GFETs using a CF_4 plasma. The covalent attachment of partial fluorine groups and carbon fluoride groups to graphene could offer an opportunity for achieving some unique transport properties, and the partial doping of BCP could indirectly alter these as well. Figure 3-6a shows a shift in the neutrality point with different exposure times to CF_4 plasma. With an increase in exposure time, the neutrality point first shifted to right towards a positive value, and then shifted to left a little bit; and finally shifted to right again at longer exposure times. In this process, F, CF_2 and CF_3 radicals in the plasma play an important role in the reaction with BCP and graphene. Similar trends were observed with a total of 14 selected devices on 3 different samples (Figure 3-7).

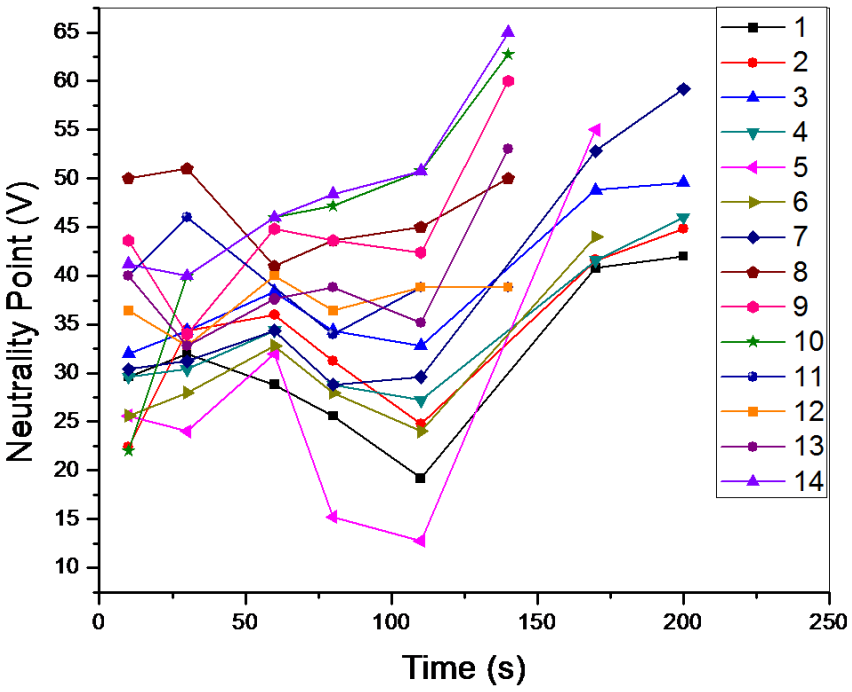

Figure 3-7 Neutrality point shift curve with different exposure time to CF_4 plasma of 14 devices. The I-V test points were 10s, 30s, 60s, 80s, 110s, 140s, 170s, 200s. [47]

Note that different devices required varying exposure times in modulating the shift of the neutrality point, perhaps because of different coverage patterns of BCP on the devices. The controllable shift mechanism could be explained by further analysing the doping effect of the particular polymer. Initially, polymer chains could be destroyed by forming C-F bonds, which introduce electron acceptors thus causing a p-type doping. Chen et al.[42] reported that electron transfer from graphene to adsorbed tetrafluorotetracyanoquinodimethane ((F4-TCNQ) is responsible for the p-type doping of graphene. In our case, the chain C-F bonds formed during the plasma treatment acted in the same manner. With increasing the treatment time, the benzyl and pyridine groups react further with the CF_4 plasma, introducing more electron acceptors, and the neutrality point then shifts further to more positive

values. Another possibility is that the flurocarbon polymer may have formed on the surface of BCP which will indirectly cause p-type doping in graphene. The disappearance of these two functional groups enable restoring of the pristine graphene properties, hence the subsequent reverse shift of the neutrality point is observed. Figure 3-6b shows the normalized conductance-gate voltage curves obtained for different plasma exposure times. It is observed that with increasing exposure time, the electron conduction is preserved, whereas the hole conduction is altered significantly. During the plasma reaction process, it is likely to have more dangling bonds generated in polymer chains that are producing positive/negative charges which may induce a n/p-type doping effect. Considering the complexity of the experimental system, it is very difficult to pinpoint whether positively or negatively charged molecules are produced. Together with the charged molecules and the electron accepting characteristic of the CFx group on the device, an increase in the hole mobility was observed. When the exposure time was increased from 10s to 110s , the hole mobility increased from 440 $cm^2/V{\cdot}s$ to 724 $cm^2/V{\cdot}s$. AFM images taken after a 110s of CF_4 plasma treatment show that the domains of PS and P4VP are not clear any more. This further clarifies the reaction mechanism. Moreover, the minimum neutrality point couldn't be returned to the value of that of pristine graphene because of the doping effect of the fluorinated polymer. These results point to a general route for tuning the transport properties of polymer-coated graphene; theoretically, any kind of polymer could be doped with fluorine which

will produce a polymer with fluorine groups and this could further change the transport properties of graphene layers.

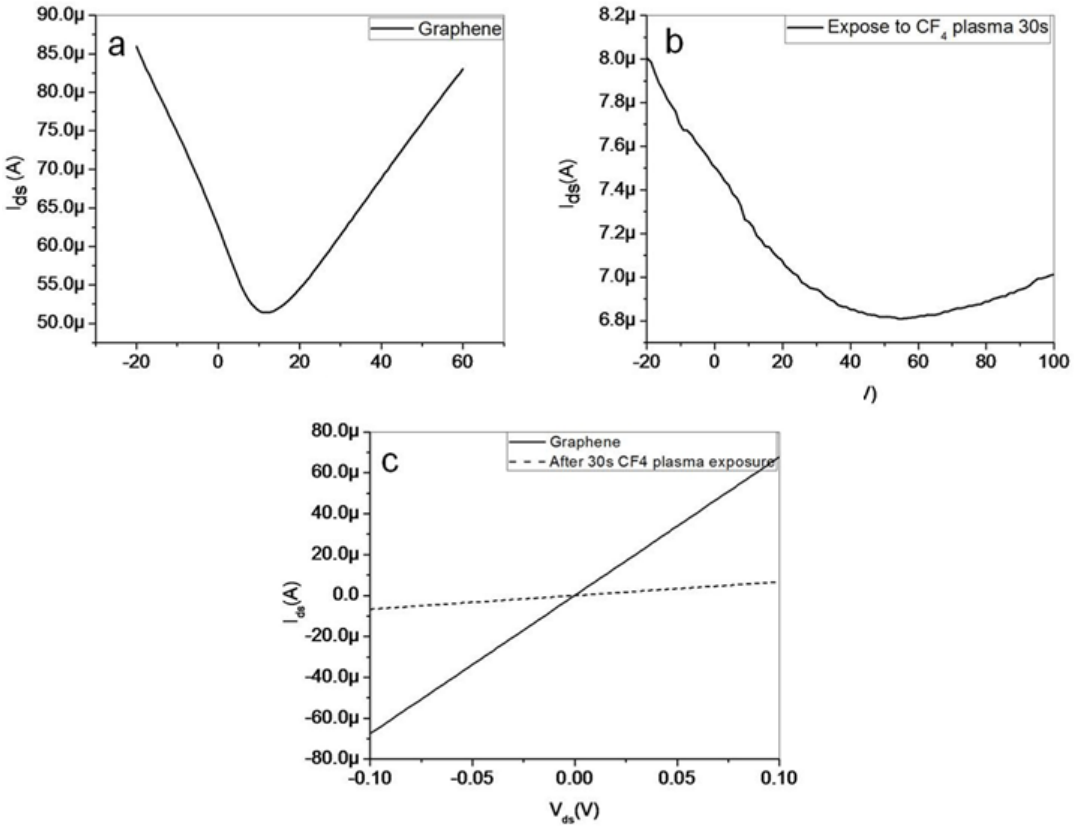

Figure 3-8 Typical source-drain current vs gate voltage (I_{ds}-V_g) curves of control sample of pristine graphene before (a) and after 30s CF_4 plasma treatment (b), And (c) I_{ds}-V_{ds} curves of these two smaples which show the one order increase of resistivity after 30s plasma treatment. [47]

When the time of exposure of our samples to the CF_4 plasma was increased to 170s, the neutality point shifted towards right significantly, presumably because of direct doping of graphene with F, CF_2 or CF_3 radicals. The BCP-ordered structures were completely removed when the time increased to 200s, but the corresponding AFM image shows that some residues still remain on the graphene surface which

could display a p-type doping effect (Figure 3-2c). The loss of the protective layer should at the same time introduce more chances of F doping on the graphene and further decrease its conductivity. The need for this harsh treatment to remove the BCP demonstrates the stability of the BCP layer, which indicates that such BCP could be utilized as a protective layer for other applications, such as biochemical sensors. A control experiment was conducted by exposing the device without a BCP layer to plasma treatment for 10s, during which 60% of the devices weren't conductive anymore and those which preserved their conductivty had a high positive neutrality point value (Figure 3-8). The minimum value of conductance increased from 5×10^{-5}S to 6.8×10^{-5}S after plasma processing. This result further ractifies the significant role that BCP could play both as a protective layer and a doping layer to GFETs.

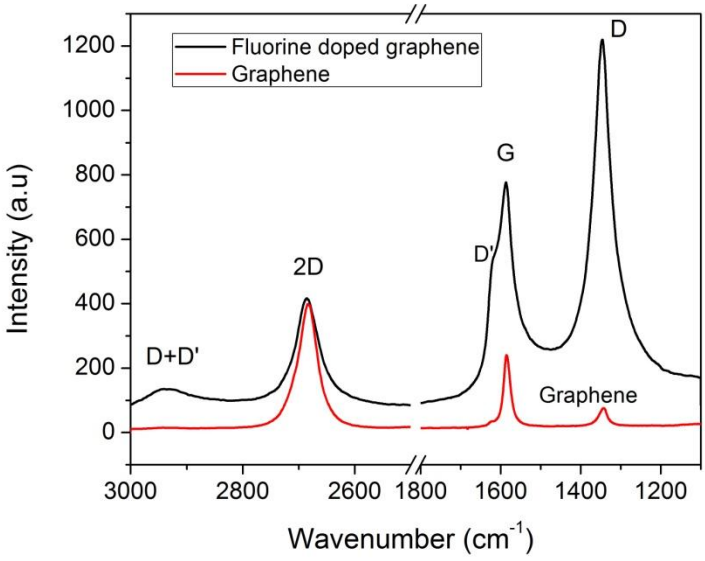

Figure 3-9 Raman spectra of graphene and fluorine doped graphene with CF4 plasma treatment for 10s. [47]

3.4 Characterization of Chemical and Strctural Properties of Doped Graphene

To further examine the doping effect of fluorine to CVD grown graphene sheets, both x-ray photoelectron spectroscopy (XPS) and Raman spectroscopy data were taken for blank graphene and for graphene exposed to CF_4 plasma for 10s. The reactive ion plasma etching conditions used here were the same as in the doping experiments disscussed above. It is clear that the intensity of the D peak of fluorinated graphene is much larger than that of the G and 2D peaks (Figure 3-9). As the D resonance requires a defect for its activation, its presence is associated with an increased degree of disorder. Several studies on carbon nanotube and carbon bulk materials showed that sp^3 bond which is produced from breaking of the sp^2 network in graphene contributes to D peak intensity increase. The XPS study further confirms the existence of significant amounts of F in the films after plasma treatment (Figure 3-10).

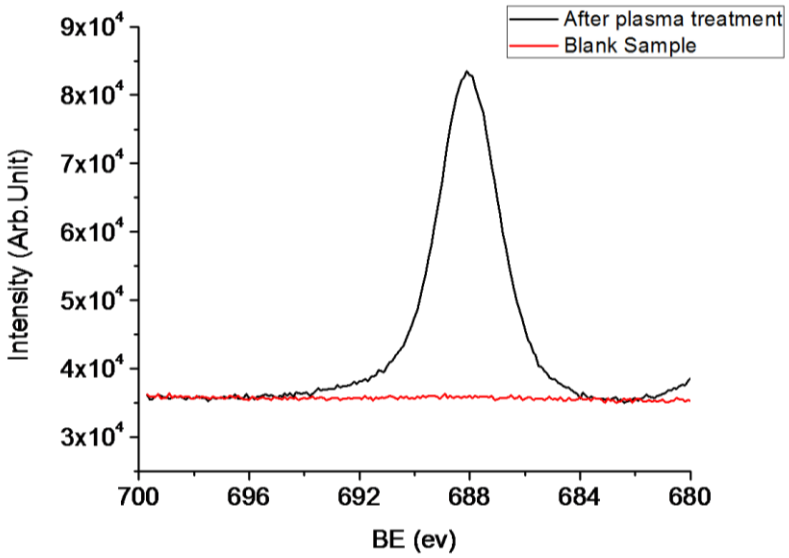

Figure 3-10 F 1s XPS spectra from a blank graphene sample (red traces) and from a sample after a CF_4 plasma treatment for 10s (black traces). [47]

Interestingly, the total intensity of C drops while the intensities of O and Si (from the underlying substrate) increase (Figure 3-11).

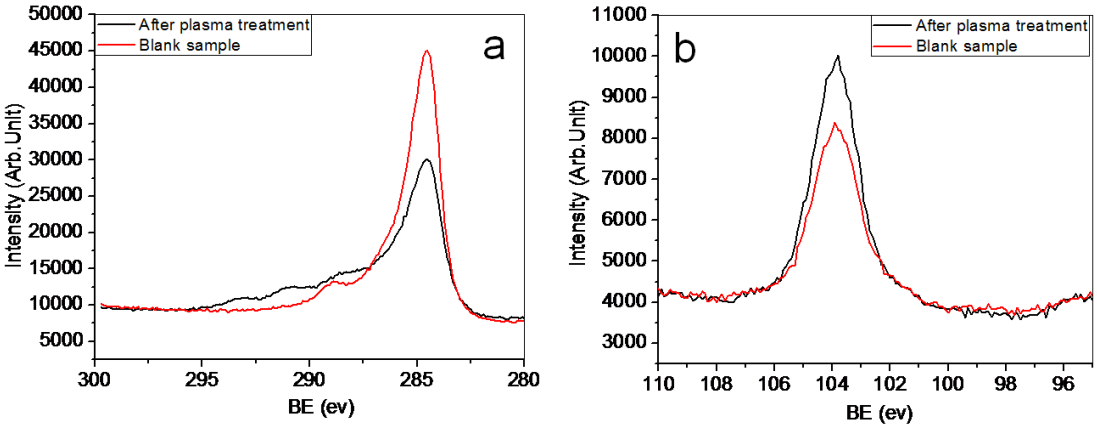

Figure 3-11 Plots the XPS spectra of (a) C 1s and (b) Si 2p. [47]

This may be caused by partial removal of the graphene layer during plasma processing. Deconvolution of the C 1s peak, following a procedure similar to that

reported in the literature[38,41], was carried out to better identify the carbon species present on the surface. Plots of the fittings of the C peaks are shown in figure 3-12, and the resulting peak areas, peak positions, and assignments are listed in Tables 1 and 2. It was determined that a 10s exposure of graphene to the CF_4 plasma results in high levels of F doping. Based on the measured area and atomic sensitivity factor of F (1s) and C(1s), the estimated F/C ratio is approximately 56%.

Table 3-1 The peak positions, peak areas, and assignments obtained from blank sample fittings. [47]

	Peak 1	Peak 2	Peak 3	Peak 4
Position (eV)	**284.6**	**286.3**	**287.9**	**289.3**
Area (%)	**68**	**19**	**7**	**6**
Assignment	**C-C**	**C-O**	**C=O**	**C(O)O**

Table 3-2 The peak positions, peak areas, and assignments obtained from F-doped sample fittings. [47]

	Peak 1	Peak 2	Peak 3	Peak 4	Peak 5	Peak 6
Position	**284.6**	**286.3**	**287.9**	**289.3**	**291.1**	**293.2**
Area (%)	**51**	**17**	**12**	**8**	**8**	**4**
Assignment	**C-C**	**C-O**	**C=O or C-CF_3**	**C(O)O Or C-F**	**C-F_2**	**C-F_3**

It has to be noted that the CF_4 plasma itself could introduce carbon atoms which indicates the probable higher ratio of doping F for graphene. These doping effects are strong enough to break the honeycomb structure of graphene, which would lead to the decrease in conductivity indicated by our electrical conductivity survey (Figure 3-8). In fact, a significant fraction of the fluorine is found in CF_3 and CF_2 moieties, proving that there is some degree of sp^2 to sp^3 carbon hybridization conversion in the graphene upon plasma treatment. The presence of C=O bonds in the blank sample also demonstrates a p-type doping behavior of the sample, a possible reason for the positive shift of the neutrality point after the sample is exposed to air.

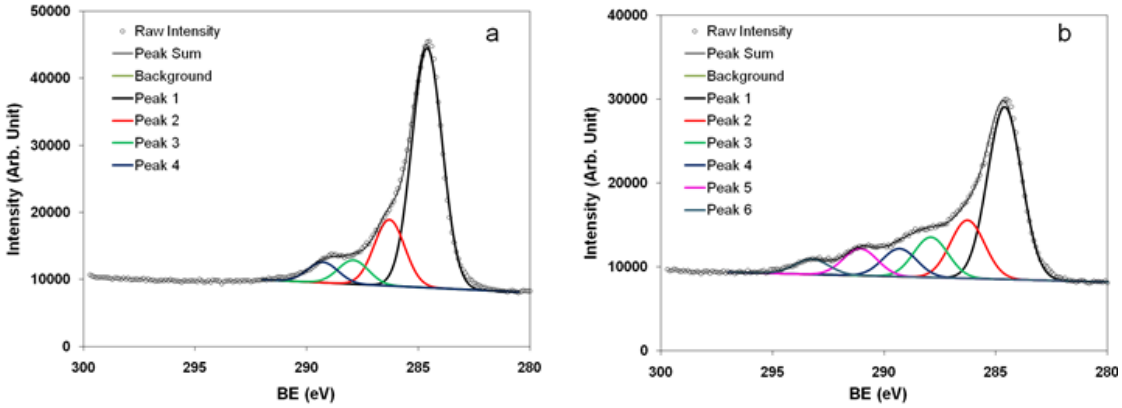

Figure 3-12 Plots of the fittings for the C is XPS peak obtained from the (a) blank and (b) 10s CF_4 plasma-exposed samples. [47]

3.5 References

[1] K. S. Novoselov, A. K. Geim, S. V. Morozov, D. Jiang, Y. Zhang, S. V. Dubonos, I. V. Grigorieva, A. A. Firsov, Science 2004, 306, 666.

[2] M. J. Allen, V. C. Tung, L. Gomez, Z. Xu, L. M. Chen, K. S. Nelson, C. W. Zhou, R. B. Kaner, Y. Yang, Adv. Mater. 2009, 21, 2098.

[3] E. J. H. Lee, K. Balasubramanian, R. T. Weitz, M. Burghard, K. Kern, Nature Nanotech. 2008, 3, 486.

[4] F. Wang, Y. B. Zhang, C. S. Tian, C. Girit, A. Zettl, M. Crommie, Y. R. Shen, Science 2008, 320, 206.

[5] P. Avouris, Z. H. Chen, V. Perebeinos, Nature Nanotech. 2007, 2, 605.

[6] X. L. Li, X. R. Wang, L. Zhang, S. W. Lee, H. J. Dai, Science 2008, 319, 1229.

[7] X. T. Jia, M. Hofmann, V. Meunier, B. G. Sumpter, J. Campos-Delgado, J. M. Romo-Herrera, H. B. Son, Y. P. Hsieh, A. Reina, J. Kong, M. Terrones, M. S. Dresselhaus, Science 2009, 323, 1701.

[8] L. Y. Jiao, L. Zhang, X. R. Wang, G. Diankov, H. J. Dai, Nature 2009, 458, 877.

[9] J. W. Bai, X. Zhong, S. Jiang, Y. Huang, X. F. Duan, Nature Nanotech. 2010, 5, 190.

[10] T. Ohta, A. Bostwick, T. Seyller, K. Horn, E. Rotenberg, Science 2006, 313, 951.

[11] X. R. Wang, X. L. Li, L. Zhang, Y. Yoon, P. K. Weber, H. L. Wang, J. Guo, H. J. Dai, Science 2009, 324, 768.

[12] S. Y. Zhou, G. H. Gweon, A. V. Fedorov, P. N. First, W. A. De Heer, D. H. Lee, F. Guinea, A. H. C. Neto, A. Lanzara, Nature Mater. 2007, 6, 770.

[13] J. H. Chen, C. Jang, S. Adam, M. S. Fuhrer, E. D. Williams, M. Ishigami, Nature Phy. 2008, 4, 377.

[14] H. Lee, J. Ihm, M. L. Cohen, S. G. Louie, Nano Lett. 2010, 10, 793.

[15] I. Gierz, C. Riedl, U. Starke, C. R. Ast, K. Kern, Nano Lett. 2008, 8, 4603.

[16] X. C. Dong, D. L. Fu, W. J. Fang, Y. M. Shi, P. Chen, L. J. Li, Small 2009, 5, 1422.

[17] D. B. Farmer, R. Golizadeh-Mojarad, V. Perebeinos, Y. M. Lin, G. S. Tulevski, J. C. Tsang, P. Avouris, Nano Lett. 2009, 9, 388.

[18] L. S. Panchokarla, K. S. Subrahmanyam, S. K. Saha, A. Govindaraj, H. R. Krishnamurthy, U. V. Waghmare, C. N. R. Rao, Adv. Mater. 2009, 21, 4726.

[19] S. S. Yu, W. T. Zheng, Q. Jiang, Ieee Trans. Nanotech. 2010, 9, 78.

[20] D. C. Wei, Y. Q. Liu, Y. Wang, H. L. Zhang, L. P. Huang, G. Yu, Nano Lett. 2009, 9, 1752.

[21] I. V. Lightcap, T. H. Kosel, P. V. Kamat, Nano Lett. 2010, 10, 577.

[22] E. Bekyarova, M. E. Itkis, P. Ramesh, C. Berger, M. Sprinkle, W. A. de Heer, R. C. Haddon, J. Am. Chem. Soc. 2009, 131, 1336.

[23] Q. M. Yan, B. Huang, J. Yu, F. W. Zheng, J. Zang, J. Wu, B. L. Gu, F. Liu, W. H. Duan, Nano Lett. 2007, 7, 1469.

[24] B. J. Kim, H. Jang, S. K. Lee, B. H. Hong, J. H. Ahn, J. H. Cho, Nano lett. 2010, 10.

[25] C. Attaccalite, L. Wirtz, M. Lazzeri, F. Mauri, A. Rubio, Nano Lett. 2010, 10, 1172.

[26] H. Otsuka, Y. Nagasaki, K. Kataoka, Curr. Opin. Colloid In. 2001, 6, 3.

[27] Y. Lin, A. Boker, J. B. He, K. Sill, H. Q. Xiang, C. Abetz, X. F. Li, J. Wang, T. Emrick, S. Long, Q. Wang, A. Balazs, T. P. Russell, Nature 2005, 434, 55.

[28] Y. Ohno, K. Maehashi, Y. Yamashiro, K. Matsumoto, Nano Lett. 2009, 9, 3318.

[29] X. C. Dong, Y. Shi, W. Huang, P. Chen, L. J. Li, Adv. Mater. 2010, 22, 1.

[30] S. R. Guo, J. lin, M. Penchev, E. Yengel, C. S. Ozkan, M. Ozkan, J. Nanosci. Nanotech. 2011, 11, 5258.

[31] F. Schedin, A. K. Geim, S. V. Morozov, E. W. Hill, P. Blake, M. I. Katsnelson, K. S. Novoselov, Nature Mater. 2007, 6, 652.

[32] V. Dua, S. P. Surwade, S. Ammu, S. R. Agnihotra, S. Jain, K. E. Roberts, S. Park, R. S. Ruoff, S. K. Manohar, Angew Chem. Int. Edit. 2010, 49, 2154.

[33] Y. P. Dan, Y. Lu, N. J. Kybert, Z. T. Luo, A. T. C. Johnson, Nano Lett. 2009, 9, 1472.

[34] S. Park, J. Y. Wang, B. Kim, T. P. Russell, Nano Lett. 2008, 8, 1667.

[35] Y. Xuan, J. Peng, L. Cui, H. F. Wang, B. Y. Li, Y. C. Han, Macromol. 2004, 37, 7301.

[36] S. H. Kim, M. J. Misner, T. Xu, M. Kimura, T. P. Russell, Adv. Mater. 2004, 16, 226.

[37] C. Lee, S. H. Kim, T. P. Russell, Macromol Rapid Comm 2009, 30, 1674.

[38] P. L. Levesque, S. S. Sabri, C. M. Aguirre, J. Guillemette, M. Siaj, P. Desjardins, T. Szkopek, R. Martel, Nano Lett., 11, 132.

[39] A. K. Geim, K. S. Novoselov, Nature Mater. 2007, 6, 183.

[40] T. Shirasaki, F. Moguet, L. Lozano, A. Tressaud, G. Nanse, E. Papirer, Carbon 1999, 37, 1891.

[41] S. B. Bon, L. Valentini, R. Verdejo, J. L. G. Fierro, L. Peponi, M. A. Lopez-Manchado, J. M. Kenny, Chem. Mater. 2009, 21, 3433.

[42] W. Chen, S. Chen, D. C. Qi, X. Y. Gao, A. T. S. Wee, J. Am. Chem. Soc. 2007, 129, 10418.

[43] X. S. Li, W. W. Cai, J. H. An, S. Kim, J. Nah, D. X. Yang, R. Piner, A. Velamakanni, I. Jung, E. Tutuc, S. K. Banerjee, L. Colombo, R. S. Ruoff, Science 2009, 324, 1312.

[44] H. Tiznado, F. Zaera, J. Phys. Chem. B 2006, 110.

[45] Briggs. D, M. P. Seah, Vol. 1, John Wiley and Sons, Chichester, UK 1990.

[46] J. Lin, G. X. Liu, X. Jing, D. Teweldebrhan, R. Li, R. Lake, A.A. Balandin, M. Ozkan, C.S. Ozkan, Small, 2010, 6, 1150.

[47] S.Gue, M. Ghazinejad, X. Qin, H. Sun, W. Wang, F. Zaera, C. S. Ozkan and M. Ozkan, , Small, 2012, 8, 1073–1080,

Chapter 4

4. Conclusions

In this work after discussing the microphase separation phenomenon, block copolymers as a group of self-assembly materials with attractive technological features have been introduced. It has been demonstrated that block copolymers can offer practical pathways for manufacturing functional nanostructures. Different mechanisms to control the orientation of BCP microdomains were discussed and experimentally studied. We successfully demonstrated vertical alignment of the cylindrical diblock copolymers with neutral brush for PS-b-PMMA, and with solvent annealing, for PS-b-PnVP BCPs. The influence of polymer chain size and molecular weight in the constituent blocks were also studied by alignment and characterization PS-b-P4VP films with molecular weights ranging from 32kg/kmol to 170 kg/kmol.

Additionally, we investigated the potentials of block copolymers as platform for developing versatile functional nanostructures, including nonporous polymer

membranes, tunable arrays of metallic nanoparticles, metallic porous masks, and lithographically patterned diblock copolymer films. Our results in pattern assisted self-assembly of BCPs have demonstrated a promising route to control bottom-up self-organization processes through top-down-designed templates.

In the next section of this thesis, graphene materials and their extraordinary properties were introduced. We briefly reviewed electronic attribute of graphene as one of its greatest advantages that has been the subject of numerous research efforts. Such remarkable electronic features include high charge carrier mobility, unique band structure, and unconventional quantum hall effect. Recently, graphene-based field-effect transistors (GFETs) have been introduced as a prospect for post-silicon electronics. For fabrication of devices and interconnects, however, the electrical properties of graphene need to be modulated. Chemical doping, a major approach for tuning electronic properties, has been consistently applied in semiconductor materials to control the type and density of charge carriers.

We introduced a graphene doping strategy that is based on CF_4 plasma treatment and use of well-aligned diblock copolymers. In this approach, the graphene device is first covered by a thin film of solvent-annealed Poly (styrene-b-4-vinylpyridne) that has a cylindrical structure. Next, we demonstrated that by applying a controlled plasma assisted CF_4 doping we can control the Dirac point shift of such BCP covered GFETs. The impacts of PS and PVP chemical components, and CF_4 plasma treatment on doping characteristics were experimentally investigated. We observed that while self-assembled cylindrical diblock copolymers

can function as protective layers on GFETs, they can also modulate electron and hole conduction of graphene. When this BCP-GFET is treated with fluorine plasma doping the Dirac point could be controlled by use of different sensitivities of the PS and P4VP components of the utilized BCP. Due to the self-organizing porous structure of BCP films, the introduced BCP-GFET devices have a promising potential for sensing of gas or ions as permeable materials.